

Status epilepticus enhances tonic GABA currents and depolarizes GABA reversal potential in dentate fast-spiking basket cells

Jiandong Yu,^{1,*} Archana Proddutur,^{1,*} Fatima S. Elgammal,¹ Takahiro Ito,¹ and Vijayalakshmi Santhakumar^{1,2}

¹Department of Neurology and Neurosciences, New Jersey Medical School, University of Medicine and Dentistry of New Jersey, Newark, New Jersey; and ²Department of Pharmacology and Physiology, New Jersey Medical School, University of Medicine and Dentistry of New Jersey, Newark, New Jersey

Submitted 8 October 2012; accepted in final form 11 January 2013

Yu J, Proddutur A, Elgammal FS, Ito T, Santhakumar V. Status epilepticus enhances tonic GABA currents and depolarizes GABA reversal potential in dentate fast-spiking basket cells. *J Neurophysiol* 109: 1746–1763, 2013. First published January 16, 2013; doi:10.1152/jn.00891.2012.—Temporal lobe epilepsy is associated with loss of interneurons and inhibitory dysfunction in the dentate gyrus. While status epilepticus (SE) leads to changes in granule cell inhibition, whether dentate basket cells critical for regulating granule cell feedforward and feedback inhibition express tonic GABA currents (I_{GABA}) and undergo changes in inhibition after SE is not known. We find that interneurons immunoreactive for parvalbumin in the hilar-subgranular region express GABA_A receptor (GABA_{AR}) δ -subunits, which are known to underlie tonic I_{GABA} . Dentate fast-spiking basket cells (FS-BCs) demonstrate baseline tonic I_{GABA} blocked by GABA_{AR} antagonists. In morphologically and physiologically identified FS-BCs, tonic I_{GABA} is enhanced 1 wk after pilocarpine-induced SE, despite simultaneous reduction in spontaneous inhibitory postsynaptic current (sIPSC) frequency. Amplitude of tonic I_{GABA} in control and post-SE FS-BCs is enhanced by 4,5,6,7-tetrahydroisoazolo[5,4-c]pyridin-3-ol (THIP), demonstrating the contribution of GABA_{AR} δ -subunits. Whereas FS-BC resting membrane potential is unchanged after SE, perforated-patch recordings from FS-BCs show that the reversal potential for GABA currents (E_{GABA}) is depolarized after SE. In model FS-BCs, increasing tonic GABA conductance decreased excitability when E_{GABA} was shunting and increased excitability when E_{GABA} was depolarizing. Although simulated focal afferent activation evoked seizure-like activity in model dentate networks with FS-BC tonic GABA conductance and shunting E_{GABA} , excitability of identical networks with depolarizing FS-BC E_{GABA} showed lower activity levels. Thus, together, post-SE changes in tonic I_{GABA} and E_{GABA} maintain homeostasis of FS-BC activity and limit increases in dentate excitability. These findings have implications for normal FS-BC function and can inform studies examining comorbidities and therapeutics following SE.

interneuron; epilepsy; tonic inhibition

ACQUIRED TEMPORAL LOBE EPILEPSY occurring as a consequence of unprovoked seizures is marked by neuropathological changes in the dentate gyrus (Margerison and Corsellis 1966). Alterations in granule cell inhibition, resulting from loss or dysfunction of GABAergic interneurons, have been proposed to contribute to development of epilepsy (Cossart et al. 2005; Coulter 2001). The early period within a week after status epilepticus (SE) is characterized by enhanced entorhinal input

to the dentate gyrus (Bragin et al. 2004; Kobayashi et al. 2003) and is associated with changes in granule cell GABA currents (I_{GABA}) (Kobayashi and Buckmaster 2003; Zhan and Nadler 2009) and GABA reversal potential (E_{GABA}) (Pathak et al. 2007). The cellular and synaptic changes that occur prior to development of spontaneous seizures have been the focus of several studies because of their potential to contribute to the epileptogenic process rather than being a side effect of epilepsy (Brooks-Kayal et al. 1998; Kobayashi et al. 2003; Pathak et al. 2007). SE leads to loss and structural reorganization of interneurons and alterations in their excitatory inputs (Zhang and Buckmaster 2009; Zhang et al. 2009). Although interneuronal inhibition underlies generation of brain rhythms and regulates network activity levels (Buzsaki 2006), whether interneuronal inhibition shows early changes after SE remains untested.

Fast-spiking basket cells (FS-BCs), a class of interneurons with perisomatic projections, are critical for maintaining the low excitability and sparse firing of dentate granule cells and contribute to feedforward and feedback dentate inhibition (Ewell and Jones 2010; Kraushaar and Jonas 2000). Dentate FS-BCs express the calcium-binding protein parvalbumin (PV), have a characteristic high-frequency nonadapting firing pattern (Harney and Jones 2002; Hefft and Jonas 2005), and are interconnected through high-fidelity GABAergic synapses (Bartos et al. 2001). Apart from synaptic GABA_A receptors (GABA_{ARs}), granule cells and certain interneurons express extra- and perisynaptic high-affinity GABA_{ARs} that contribute to “tonic” I_{GABA} (Farrant and Nusser 2005; Scimemi et al. 2005). GABA_{ARs} containing δ -subunits contribute to tonic I_{GABA} in dentate granule cells and molecular layer interneurons (Glykys et al. 2007; Mtchedlishvili and Kapur 2006; Wei et al. 2003). Previous studies have shown that nonprincipal neurons in the dentate hilus express GABA_{AR} δ -subunits (Peng et al. 2004); however, whether dentate FS-BCs express tonic I_{GABA} is not known. Since tonic I_{GABA} regulates neuronal excitability and can undergo activity-dependent changes during synaptic GABA spillover (Glykys and Mody 2007), the presence of tonic I_{GABA} in FS-BCs will impact their function during network activity. Moreover, FS-BC tonic I_{GABA} may be altered after SE, as has been observed in granule cells (Zhan and Nadler 2009; Zhang et al. 2007).

GABAergic inhibition is hyperpolarizing when E_{GABA} is negative to neuronal resting membrane potential (RMP) and shunting when E_{GABA} is close to RMP. Hippocampal and dentate interneuronal E_{GABA} has been shown to lie positive to RMP, contributing to shunting inhibition (Banke and McBain

*J. Yu and A. Proddutur contributed equally to this work.

Address for reprint requests and other correspondence: V. Santhakumar, Dept. of Neurology and Neurosciences, UMDNJ-New Jersey Medical School, MSB-H 512, 185 S. Orange Ave. Newark, NJ 07103 (e-mail: santhavi@umdnj.edu).

2006; Vida et al. 2006). Curiously, whether SE alters interneuronal E_{GABA} , as was demonstrated in granule cells (Pathak et al. 2007), is not known. Interactions between GABA conductance (g_{GABA}) and E_{GABA} determine the net effect of tonic I_{GABA} on neuronal excitability (Song et al. 2011). Therefore, we examined whether dentate FS-BCs express tonic I_{GABA} and whether FS-BC tonic I_{GABA} and E_{GABA} are altered 1 wk after SE. Using single-cell models and large-scale network simulations, we characterized how the experimentally identified post-SE changes in FS-BC tonic inhibition influence FS-BC and dentate network activity.

MATERIALS AND METHODS

Pilocarpine status epilepticus. All procedures were performed under protocols approved by the University of Medicine and Dentistry of New Jersey Institutional Animal Care and Use Committee. Pilocarpine injection was performed as previously reported (Zhang et al. 2009). Young adult male Wistar rats between postnatal days 25 and 27 were injected with scopolamine methyl nitrate (1 mg/kg sc) 30 min before pilocarpine injection. SE was induced by injection of pilocarpine (300 mg/kg ip). After 1 h and 30 min of continuous stage 3 or greater seizures (Racine scale), diazepam (10 mg/kg ip) was administered and repeated as needed to terminate seizures. Control rats received scopolamine pretreatment followed by saline injection (ip) and diazepam after 2 h. Animals were video monitored (continuous video recording for 8 h on the day before experimentation with a PC333HR high-resolution camera coupled to a 4 Channel H.264 Pentaplex Digital Video Recorder) to rule out occurrence of spontaneous seizures. Unless otherwise stated, all anatomical and physiological studies were conducted on seizure-free rats 6–8 days after pilocarpine-SE and in age-matched, saline-injected control rats.

Slice preparation. One week (6–8 days) after saline injection or pilocarpine-induced SE, rats were anesthetized with isoflurane and decapitated. Horizontal brain slices (300 μ m for patch clamp and 400 μ m for field experiments) were prepared in ice-cold sucrose-artificial cerebrospinal fluid (sucrose-aCSF) containing (in mM) 85 NaCl, 75 sucrose, 24 NaHCO₃, 25 glucose, 4 MgCl₂, 2.5 KCl, 1.25 Na₂PO₄, and 0.5 CaCl₂ with a Leica VT1200S Vibratome (Wetzlar, Germany). The slices were sagittally bisected and incubated at 32 \pm 1°C for 30 min in a submerged holding chamber containing an equal volume of sucrose-aCSF and recording aCSF and subsequently held at room temperature (RT). The recording aCSF contained (in mM) 126 NaCl, 2.5 KCl, 2 CaCl₂, 2 MgCl₂, 1.25 Na₂PO₄, 26 NaHCO₃, and 10 D-glucose. All solutions were saturated with 95% O₂-5% CO₂ and maintained at a pH of 7.4 for 1–6 h.

In vitro electrophysiology. For patch-clamp recordings, slices (300 μ m) were transferred to a submerged recording chamber and perfused with oxygenated aCSF at 33 \pm 1°C. Whole cell voltage- and current-clamp recordings from interneurons at the border of the hilus and granule cell layer were performed with IR-DIC visualization techniques with a Nikon Eclipse FN-1 microscope, using a \times 40 water-immersion objective. Recordings were obtained with Axon Instruments MultiClamp 700B (Molecular Devices, Sunnyvale, CA). Data were low-pass filtered at 3 kHz, digitized with DigiData 1440A, and acquired with pCLAMP 10 at 10-kHz sampling frequency. Tonic and synaptic I_{GABA} were recorded in perfusing aCSF containing the glutamate receptor antagonist kynurenic acid (KyA, 3 mM; Tocris, Ellisville, MO). No additional GABA was included in the recording solution. Except in experiments presented in Fig. 5D, GABA transporter antagonists were not included in the recording solution. Recordings were obtained with microelectrodes (5–7 M Ω) containing (in mM) 125 KCl, 10 K-gluconate, 10 HEPES, 2 MgCl₂, 0.2 EGTA, 2 Na-ATP, 0.5 Na-GTP, and 10 phosphocreatine titrated to a pH of 7.25 with KOH. Biocytin (0.2%) was included in the internal solution for post hoc cell identification (Santhakumar et al. 2010). Recorded

neurons were initially held at -70 mV, and the responses to 1.5-s positive and negative current injections were examined to determine active and passive characteristics. Cells with nonadapting, high-frequency firing for the entire duration of the current injection and low input resistance (R_{in}) (<150 M Ω) were classified as FS-BCs (Hefft and Jonas 2005). Neurons with adapting firing, high R_{in} (>150 M Ω), and sag during negative current injection were considered non-fast-spiking interneurons (non-FS-INS) (Hefft and Jonas 2005). Post hoc biocytin immunostaining and morphological analysis were used to definitively identify FS-BCs included in this study, on the basis of presence of axon terminals in the granule cell layer. After current-clamp recordings, cells were held in voltage clamp at -70 mV for analysis of GABA currents. Tonic I_{GABA} , steady-state currents blocked by the GABA_AR antagonist SR95531 (10 μ M), was measured as described previously (Gupta et al. 2012) with custom macros in IGOR Pro 7.0 software (WaveMetrics, Lake Oswego, OR). Briefly, the magnitude of tonic I_{GABA} was calculated by plotting all-point histograms of relevant 30-s segments of data. These data were fit to Gaussian equations, constraining fits to values two bins more negative than the peak. This ensured that the tail of higher-amplitude values [representing spontaneous inhibitory postsynaptic currents (sIPSCs)] did not influence the fit (Santhakumar et al. 2006, 2010). Recordings were discontinued if series resistance increased by >20%. Cell capacitance was measured with the automated function in Multiclamp 700B. In some experiments, 4,5,6,7-tetrahydroisoxazolo[5,4-c]pyridin-3-ol (THIP, 1 μ M), a selective GABA_AR agonist with a preference for δ -subunit-containing GABA_ARs (Brown et al. 2002), or the GABA transporter-1 uptake inhibitor 1-[2-[(diphenylmethylene)imino]oxyethyl]-1,2,5,6-tetrahydro-3-pyridinecarboxylic acid hydrochloride (NO-711, 10 μ M) was included in the external solution. Individual sIPSCs were detected with custom software in IGOR Pro 7.0 (Gupta et al. 2012; Santhakumar et al. 2010). Events were visualized, and any “noise” that spuriously met trigger specifications was rejected. Cumulative probability plots of sIPSC parameters were constructed with IGOR Pro by pooling an equal number of sIPSCs from each cell.

Gramicidin-perforated-patch recordings were performed to prevent alteration of the intracellular chloride concentration by the pipette solution (Ebihara et al. 1995). Intracellular solution contained (mM) 135 KCl, 0.5 CaCl₂, 5 Na₂EGTA, 10 HEPES, 2 MgCl₂, and 2 Mg ATP, with 0.2% biocytin, pH set to 7.2 with KOH and gramicidin D (100 μ g/ μ l with 1% DMSO final concentration). Electrode tips were filled with gramicidin-free internal solution and back-filled with the solution containing gramicidin D. On formation of perforated patch, responses to positive and negative current injections were recorded in cell-attached mode for physiological identification. A cocktail containing tetrodotoxin (TTX, 1 μ M), 6,7-dinitroquinoxaline-2,3-dione (DNQX, 20 μ M), and D-(–)-2-amino-5-phosphonopentanoic acid (APV, 50 μ M) (Tocris), to block Na⁺ channels, AMPA receptors, and NMDA receptors, was used to isolate I_{GABA} . Perforated-patch recordings were obtained after series resistance had stabilized between 80 and 100 M Ω , ~40 min after patch formation. Series resistance was monitored at 2-min intervals, and data were rejected when resistance suddenly decreased, indicating rupture of the perforated patch. In some initial experiments Alexa Fluor 488 (50–100 μ M) was included in the pipette to confirm that the change in resistance was a reliable and adequate indicator of patch rupture. A Picospritzer (PMI-100, Dagan) was used to apply GABA (100 μ M, containing blockers of synaptic transmission mentioned above) at 10 psi from a pipette resting 10–20 μ m above the slice at the position of the recorded soma. Voltage ramps –130 to +10 mV over 200 ms applied from a holding potential of –60 mV in the absence and presence of GABA were used to determine E_{GABA} . The membrane voltage at which the current traces, obtained in the presence and absence of GABA, crossed was measured as the apparent E_{GABA} (Billups and Attwell 2002). RMP was measured as the potential at which holding current = 0 pA. All measurements were corrected for a liquid junction potential and

voltage drop across series resistance. In a subset of cells, E_{GABA} was also estimated by systematically varying the steady-state holding potential and estimating the reversal potential of GABA-evoked currents (Verheugen et al. 1999). After rupture of the patch, cells were filled and processed for biocytin immunostaining and morphological identification. Cells in which the access after patch rupture was inadequate were repatched with a gramicidin-free internal solution for biocytin fill. Tight-seal cell-attached recordings were obtained from FS-BCs with electrodes containing the gramicidin-free KCl-based internal solution in standard aCSF. Recordings were obtained in current-clamp mode with zero current injection. At the end of the recordings, the patch was ruptured to gain whole cell access for physiological identification and biocytin filling for post hoc morphological identification.

Field recordings were performed in an interface recording chamber (BSC2, AutoMate Scientific, Berkeley, CA) perfused with aCSF. Brain slices (400 μ m) rested on filter paper and were stabilized with platinum wire weights. The tissue was continuously superfused with humidified 95% O₂-5% CO₂, and the temperature of the perfusing solution was maintained at 34°C with a proportional control heating unit (PTC03, AutoMate Scientific). Field recordings of evoked population spikes in the granule cell layer of the dentate gyrus were obtained with patch pipettes filled with recording aCSF. To evoke the field responses, constant-current stimuli (0.5–4 mA, 50 μ s) were applied at 0.1 Hz through a bipolar 90- μ m tungsten stimulating electrode placed in the perforant path, at the junction of the dorsal blade and the crest just outside the fissure where it was visualized as a fiber tract (Gupta et al. 2012; Santhakumar et al. 2001), and coupled to a high-voltage stimulus isolator (A365R, WPI, Sarasota, FL). Recordings were obtained with an AxoPatch200B amplifier, filtered at 4 kHz with a Bessel filter, and digitized at 10 kHz with a DigiData 1440A analog-digital interface (Molecular Devices). The field responses in the granule cell layer were measured at five predetermined points in each slice (Santhakumar et al. 2000), including the tips of the dorsal and the ventral blades, the middle of the dorsal and ventral blades, and the middle of the crest, and the largest response was studied further. All salts were purchased from Sigma-Aldrich (St. Louis, MO).

Anatomical methods. NeuN staining was performed on sections from rats perfused with 4% paraformaldehyde 1 wk after pilocarpine-induced SE and from age-matched, saline-injected control rats. Sections (40 μ m) were incubated overnight at RT with anti-NeuN antibody (MAB377, 1:10,000, mouse monoclonal; Millipore) in 0.3% Triton X-100 and 2% normal goat serum (NGS) in phosphate-buffered saline (PBS). Sections were reacted with Alexa Fluor 594-conjugated goat anti-mouse secondary to reveal staining. Quantification was performed on every 11th section along the septo-temporal extent of the hippocampus. Cell counts were performed with the optical fractionator of Stereo Investigator V.10.02 (MBF Bioscience, Williston, VT) on an Olympus BX51 microscope with a $\times 100$ oil objective. In each section, the hilus was outlined by a contour traced with a $\times 10$ objective. Sampling parameters were set at 100 \times : counting frame = 50 μ m \times 50 μ m, dissector height = 30 μ m, and top guard zone = 5 μ m. Approximately 25 sites per contour were selected with randomized systematic sampling protocols in Stereo Investigator (West et al. 1991).

Immunohistological studies were performed in rats perfused 1 wk after SE and in age-matched control rats. Sections were selected at random from the entire septo-temporal extent of the hippocampus. Sections were processed for antigen retrieval in a water bath (Peng et al. 2004). Briefly, free-floating sections were incubated in 0.05 M sodium citrate solution, pH 6.0 at RT (30 min), and subsequently heated in a water bath at 90°C for 30 min. Sections were allowed to cool at RT for 30 min and rinsed in PBS. Sections were processed for double immunofluorescence labeling for GABA_AR δ -subunit or KCC2 and PV. After antigen retrieval, sections were blocked with 10% NGS and 0.3% Triton X-100 in PBS at RT for 1 h and incubated

in a solution containing rabbit anti- δ (1:200; 868-GDN, PhosphoSolutions) and monoclonal mouse anti-PV (1.5:1,000; 235, Swant) in PBS with 0.3% Triton X-100 and 2% NGS at RT for 24 h. Sections were rinsed in PBS and incubated at 4°C for 24 h in a mixture of goat anti-rabbit IgG conjugated to Alexa Fluor 488 (1:250) to reveal GABA_AR δ -subunit and goat anti-mouse labeled with Alexa Fluor 594 (1:500) to reveal PV. Similar procedures were used to examine double labeling for KCC2 and PV with polyclonal rabbit anti-KCC2 (1:200; Millipore) and monoclonal mouse anti-PV (1.5:1,000; 235, Swant) and appropriate secondary antibodies. Sections were rinsed in PBS and mounted with Vectashield (Vector Labs). Controls in which primary antibody was omitted were routinely included. Additionally, sections from mice lacking the GABA_AR δ -subunit (*Gabrd*^{-/-} mice, a generous gift from Dr. Jamie Maguire, Tufts University) were used to confirm specificity of the GABA_AR δ -subunit primary antibody. Double labeling was quantified in the granule cell layer and 100 μ m of the subgranular region of the hilus. The region of interest (ROI) was outlined by a contour traced with a $\times 10$ objective. Sampling parameters were set at 100 \times : counting frame = 100 μ m \times 60 μ m, dissector height = 30 μ m, and guard zones = 5 μ m. In each section, an observer marked the outline of PV-positive (PV+) somata in the ROI under epifluorescence illumination and a $\times 100$ oil objective and switched filters to visually examine the expression of GABA_AR δ -subunit in the PV-labeled soma. Neurons were deemed colabeled if the staining for GABA_AR δ -subunit shared the outline of the PV-labeled soma and had a greater intensity than the hilar neuropil. The percentage of PV-labeled cells that were colabeled for GABA_AR δ -subunit was determined. Single-plane confocal images for illustration were obtained with a Nikon A1R laser confocal microscope with a $\times 60$ water objective and identical camera settings. Semiquantitative analysis of GABA_AR δ -subunit and KCC2 fluorescence intensity in PV+ neurons was performed on images from an equal number of randomly selected PV+ neurons in the hilar-granule cell layer border from each section. Images were obtained with a Nikon A1R laser confocal microscope with a 1.2 NA $\times 60$ water objective with identical camera settings and converted to RGB color mode. An ROI was traced around PV+ neurons (in the red channel), and the average grayscale intensity of GABA_AR δ -subunit was determined in the green channel (δ -subunit). For estimation of KCC2 fluorescence intensity in PV+ neurons, the ROI was confined to the periphery of the PV-labeled profile in order to assess membrane expression of KCC2. Image analysis was performed with ImageJ v1.43u (National Institutes of Health) by an investigator blind to the treatment.

After physiological recordings, slices were fixed in 0.1 M phosphate buffer containing 4% paraformaldehyde at 4°C for 2 days. For post hoc immunohistochemistry, thick slices (300 μ m) were incubated overnight at RT with anti-PV antibody (PV-28, 1.5:1,000, polyclonal rabbit, Swant) in 0.3% Triton X-100- and 2% NGS-containing PBS. Immunoreactions were revealed with Alexa Fluor 488-conjugated secondary goat antibodies against rabbit IgG (1:250), and biocytin staining was revealed with Alexa Fluor 594-conjugated streptavidin (1:1,000). Sections were visualized and imaged with a Nikon A1R laser confocal microscope with a 1.2 NA $\times 60$ water objective. As a result of prolonged recordings and use of high-chloride internal solution, few cells showed somatic labeling for PV. When present, the expression of PV in the soma or dendrites was used as an added confirmation of cell identity. Cell reconstructions and morphological analyses were performed with Neurolucida V.10.02 (MBF Bioscience) and confocal image stacks.

Computational modeling. Single FS-BC models and dentate network simulations were implemented with the NEURON 7.0 simulation environment (Hines and Carnevale 1997). The biophysically realistic FS-BC model was adapted from earlier studies (Dyhrfjeld-Johnsen et al. 2007; Santhakumar et al. 2005) and included a soma and two apical and basal dendrites each with four distinct compartments (a total of 17 compartments). Active and passive conductances were distributed as detailed previously (Santhakumar et al. 2005).

Sodium and fast delayed-rectifier potassium channels were restricted to the soma and proximal dendrites. Reversal potential of a nonspecific leak channel was set to -75 mV to modify the basket cell RMP to match the data from perforated-patch recordings in the present study. Conductance of the nonspecific leak channel was not altered. Tonic g_{GABA} was modeled as a linear deterministic leak conductance with reversal (E_{GABA}) based on experimental data: -74 mV or -54 mV. Tonic g_{GABA} was distributed uniformly in all compartments and varied from 0 to 0.1 mS/cm^2 . In some simulations, tonic g_{GABA} was restricted to the soma and proximal dendrite to determine whether the distribution of tonic g_{GABA} altered the magnitude of tonic I_{GABA} or R_{in} in model FS-BCs. In simulations performed to examine the biologically relevant range of tonic g_{GABA} (see Fig. 10B), FS-BCs were simulated with a somatic voltage clamp and E_{GABA} was set to 0 mV to model symmetrical chloride of our physiological recordings. Model FS-BCs were voltage clamped at -70 mV, tonic g_{GABA} was varied between 0 and 5 mS/cm^2 , and tonic I_{GABA} was measured as the difference in baseline current in the presence and absence of tonic g_{GABA} . R_{in} was measured in response to -100-pA current injection. To examine the effect of tonic I_{GABA} on neuronal excitability, model FS-BCs were activated by identical 200-Hz Poisson-distributed trains of excitatory synaptic inputs to the apical distal dendrites. Excitatory synaptic parameters were based on AMPA conductances in previous studies (Santhakumar et al. 2005), with the synaptic AMPA conductance (g_{AMPA}) set at 3 nS to simulate low activity levels and $g_{\text{AMPA}} = 20 \text{ nS}$ to simulate high activity levels. The effect of increasing tonic g_{GABA} on evoked firing of the model FS-BC was examined with E_{GABA} set at -74 mV (control) and -54 mV (after SE).

The large-scale, topologically and biophysically constrained model network used in this study was adapted from the 500-cell network described by Santhakumar et al. (2005) and expanded to include 1,000 granule cells, 30 mossy cells, 12 basket cells, and 12 hilar interneurons. The multicompartmental single-cell models, distribution and magnitude of active and passive properties, and synaptic conductances were based on Santhakumar et al. (2005) and were derived from anatomical and physiological data in the literature. The networks were topographically constrained, incorporating the axon distribution of the cell types, and simulated by distributing the neurons in a ring structure to avoid edge effects. Enhanced excitability in the early post-SE condition was modeled by including mossy fiber sprouting, simulated by adding synaptic connections from granule cells to the proximal dendrites of granule cells. Since the simulations were designed to test early stages of network excitability (1 wk after SE), the degree of mossy fiber sprouting in the model was set at 20% of the maximal sprouting observed in the pilocarpine model of epilepsy (Dyhrfjeld-Johnsen et al. 2007). In a second set of simulations, both sprouting and hilar neuronal loss were simulated with 20% sprouting as detailed above and a corresponding deletion of 20% of randomly selected hilar mossy cells and dendritically projecting interneurons as described in earlier studies (Santhakumar 2008; Santhakumar et al. 2005). Network models were simulated with 2.5-Hz spontaneous activity in all 1,000 granule cells during the entire duration of the simulation (3,500 ms). Spontaneous activity was simulated as independent Poisson-distributed spike trains to the perforant path input (Dyhrfjeld-Johnsen et al. 2007). A single, synchronous synaptic input to 100 granule cells and 2 local basket cells (at $t = 2,001$ ms) was used to simulate focally evoked network firing. The basket cell models (and only basket cell models) included tonic g_{GABA} (described above in the single-cell model) distributed uniformly and in all compartments. In networks simulated with control GABA reversal, E_{GABA} of both tonic and synaptic GABA currents in all model FS-BCs was set to -74 mV. Similarly, networks with the post-SE depolarized GABA reversal were simulated with E_{GABA} for tonic and synaptic GABA currents in basket cells set to -54 mV. In a subset of simulations including sprouting and hilar cell loss (see Fig. 11E), E_{GABA} of synaptic and tonic g_{GABA} were set to different values. The E_{GABA} at GABA synapses on other neurons was not altered. Simulations included

"synaptic spillover," modeled to simulate increases in tonic g_{GABA} that accompany increases in extracellular GABA levels during neuronal activity (Glykys and Mody 2007). Spillover was modeled by including three "spillover GABA conductances" with progressively decreasing amplitudes associated with each inhibitory synaptic connection to model FS-BCs. The spillover GABA conductances were modeled as synapses with slower rise (7 ms) and decay time (200 ms) constants (Rossi et al. 2003) and had 20%, 10%, and 5% of the peak conductance of the primary synapse. The effect of basket cell g_{GABA} and E_{GABA} on the average frequency of granule cell spontaneous activity and evoked activity were quantified during 1,000–2,000 ms and 2,001–3,500 ms, respectively. In initial simulations, instantiation of the network connections was randomized within preset topological constraints. Each set of simulations was run multiple times, and summary data are presented as means \pm SE. In some simulations the random seed of the network connectivity was set to a specific value, and the effect of tonic g_{GABA} and E_{GABA} on dentate excitability was compared in structurally identical networks.

Analysis and statistics. Statistical analysis was performed by paired and unpaired Student's *t*-test (Microsoft Excel 2007) or Kolmogorov-Smirnov (K-S) test (in IGOR Pro 7.0) for data that were not distributed normally or univariate and multivariate repeated-measures ANOVA (Systat) for experiments involving repeated measurements from the same sample. Significance was set to $P < 0.05$. Data are shown as mean \pm SE or median and interquartile range (IQR) where appropriate.

RESULTS

Early dentate cell loss and enhanced excitability in young adult rats after status epilepticus. A single episode of SE following injection of pilocarpine leads to development of recurrent spontaneous seizures and has been used to model acquired epilepsy. In adult rats, pilocarpine-induced SE replicates the characteristic hippocampal cell loss and network reorganization observed in epileptic patients. The presence and extent of cell loss in younger rats may be variable (Raol et al. 2003). Therefore, we performed NeuN staining for neuronal nuclei in tissue from control rats and those subjected to SE to examine whether SE in the young adult rats (postnatal days 25–27) used in the present study resulted in dentate hilar cell loss. As illustrated in Fig. 1, comparison of sections prepared 1 wk after pilocarpine-induced SE (post-SE) and from age-matched saline-injected control rats revealed a significant decrease in NeuN-stained neurons in the dentate hilus after SE (Fig. 1, A and B; control: 377.5 ± 40.4 hilar neurons counted/section, a total of 4,251 cells counted in 15 sections from 3 rats; post-SE: 225.7 ± 18.8 hilar neurons counted/section, based on 2,789 cells counted in 15 sections from 3 rats; $40.2 \pm 5.0\%$ decrease, $P < 0.05$, Student's *t*-test) consistent with observations in previous studies (Kobayashi et al. 2003; Mello et al. 1993; Zhang et al. 2012). Additionally, hippocampal sections from rats 1 wk after SE but not control rats had degenerating neurons stained by Fluoro-Jade C in CA1 and CA3 (data not shown), as observed in previous studies (Ekstrand et al. 2011). These data demonstrate that the young adult rats used in the present study show hilar cell loss within a week after SE. Previous studies have identified changes in dentate excitability and granule cell inhibition 1–2 wk after SE and prior to onset of epileptic seizures (Pathak et al. 2007). We examined the population spike (Fig. 1C) of dentate granule cells in response to perforant path stimulation to determine whether dentate network excitability was altered 1 wk after SE. Field recordings showed that the amplitude of the afferent-evoked granule cell population spike was enhanced 1 wk

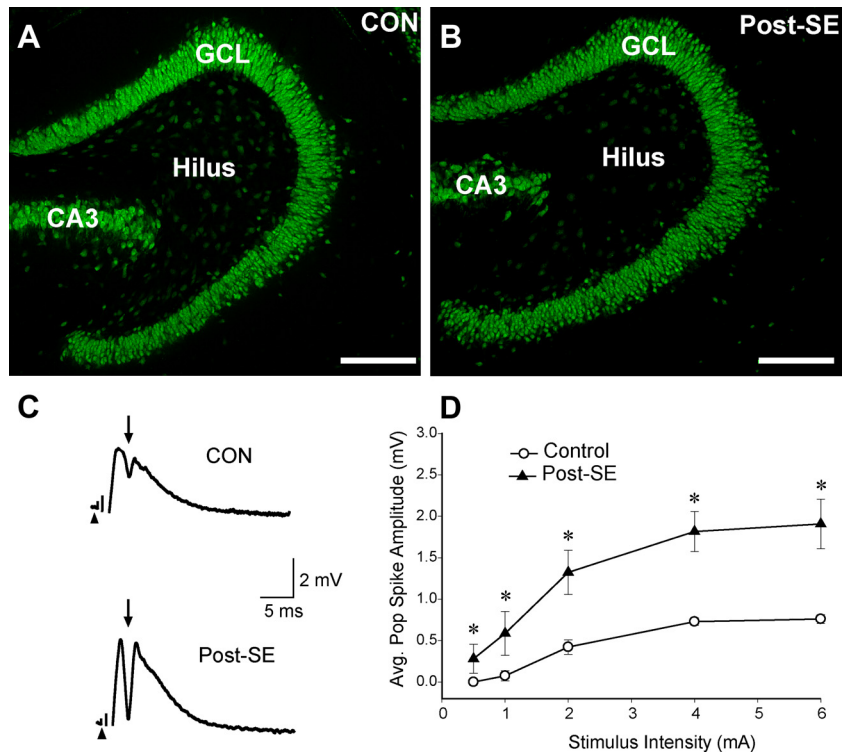


Fig. 1. Early changes in dentate network function after pilocarpine-induced status epilepticus (SE). *A* and *B*: photomicrographs of NeuN-stained sections obtained from rats perfused 1 wk after saline injection or pilocarpine-induced SE demonstrate the presence of numerous NeuN-stained hilar neurons in the section from the control (*A*) and fewer hilar NeuN-stained neurons in a level-matched post-SE section (*B*). GCL, granule cell layer. Scale bars, 200 μ m. *C*: representative traces of granule cell field responses evoked by perforant path stimulation in slices from control (*top*) and 1 wk after SE (*bottom*) illustrate the larger population spike amplitude in the post-SE dentate. Traces are an average of 4 trials in response to a 4-mA stimulus to the perforant path. Arrowheads indicate the location of the truncated stimulus artifact, and arrows point to the population spike. *D*: summary data demonstrate the post-SE increase in dentate-evoked excitability at various stimulation intensities. Error bars indicate SE. * $P < 0.05$ by repeated-measures ANOVA.

after SE compared with age-matched control rats (Fig. 1*C*). Summary data demonstrate the post-SE increase in dentate population spike amplitude at various stimulation intensities [Fig. 1*D*; control: $n = 8$ slices from 4 rats, post-SE: $n = 13$ slices from 6 rats; $F_{(1,19)} = 8.93$, $P < 0.05$ by univariate repeated-measures ANOVA]. Even when the population spike amplitude was normalized by the simultaneously recorded field excitatory postsynaptic potential (fEPSP) slope, to account for differences in effective excitatory synaptic drive in response to stimulation, the fEPSP-normalized population spike amplitude was significantly greater in slices from post-SE rats [$F_{(1,19)} = 4.8$, $P < 0.05$ by repeated-measures ANOVA]. Since identifying early SE-induced changes in dentate inhibition can provide mechanistic insights into dentate physiology in the latent period leading up to spontaneous seizures, we focused on inhibitory plasticity of perisomatically projecting PV-expressing basket cells 1 wk after SE.

GABA_AR δ-subunits are expressed in parvalbumin-positive dentate interneurons. In dentate granule cells, SE leads to alterations in synaptic and extrasynaptic GABA_AR expression and in synaptic and tonic I_{GABA} (Mtchedlishvili and Kapur 2006; Peng et al. 2004; Zhan and Nadler 2009; Zhang et al. 2007). Hippocampal and dentate interneurons appear to express GABA_ARs underlying tonic I_{GABA} and demonstrate tonic I_{GABA} (Glykys et al. 2007; Semyanov et al. 2003; Song et al. 2011). Studies in mice have revealed that GABA_AR δ-subunits, known to underlie tonic I_{GABA} , are expressed in presumed interneurons in the hilar-granule cell layer border (Peng et al. 2004). However, whether perisomatically projecting basket cells, which express PV and are critical for rapid and precise inhibition (Freund 2003; Hefft and Jonas 2005), express GABA_AR δ-subunits has not been determined. Confocal images of hippocampal sections, obtained from rats 1 wk after saline injection or pilocarpine-induced SE and immunostained for PV and GABA_AR δ-subunits, showed that PV-labeled neurons in the hilar-granule

cell layer border (Fig. 2, *A–D, right*) consistently demonstrated somatic labeling for GABA_AR δ-subunits (Fig. 2, *A* and *C, center*). The intense GABA_AR δ-subunit labeling of granule cell dendrites made it difficult to isolate GABA_AR δ-subunit labeling of PV+ dendrites in the molecular layer. However, PV+ dendrites in the hilus of both the control (Fig. 2*B*) and post-SE (Fig. 2*D*) rats showed distinct colabeling for GABA_AR δ-subunit, consistent with somato-dendritic staining for GABA_AR δ-subunit observed in other neuronal types (Olah et al. 2009; Zhang et al. 2007). Absence of immunostaining in sections from *Gabrd*^{-/-} mice lacking the GABA_AR δ-subunit was used to confirm specificity of the GABA_AR δ-subunit primary antibody (data not shown). As illustrated by the summary plots, $99.1 \pm 0.9\%$ of the 115 PV+ neurons from control rats (18 slices from 3 rats) and $97.1 \pm 2.9\%$ of the 120 PV+ neurons from post-SE rats (18 slices from 3 rats) in the hilar-granule cell layer border (see MATERIALS AND METHODS) were colabeled for GABA_AR δ-subunit (Fig. 2*E*). The proportion of PV+ neurons labeled for the GABA_AR δ-subunit was not altered after SE (Fig. 2*F*; $P > 0.05$ by Student's *t*-test). However, quantification of the fluorescence intensity for GABA_AR δ-subunit expression in PV-labeled neurons from control and post-SE rats revealed a significant increase in expression of GABA_AR δ-subunit after SE (Fig. 2*F*; grayscale intensity in arbitrary units: control 14.7 ± 5.7 , $n = 65$ cells from 3 rats; post-SE 24.2 ± 15.8 , $n = 70$ cells from 3 rats, $P < 0.05$ by Student's *t*-test). These data demonstrate expression and post-SE enhancement of GABA_AR δ-subunits in PV+ interneurons in the hilar-granule cell layer border.

Expression of tonic GABA currents in dentate fast-spiking basket cells. In light of our immunostaining data demonstrating the expression of GABA_AR δ-subunits in PV+ interneurons (Fig. 2), we examined whether PV+ basket cells express functional tonic I_{GABA} . Dentate PV+ basket cells can be distinguished from the other interneurons in the hilar-granule cell

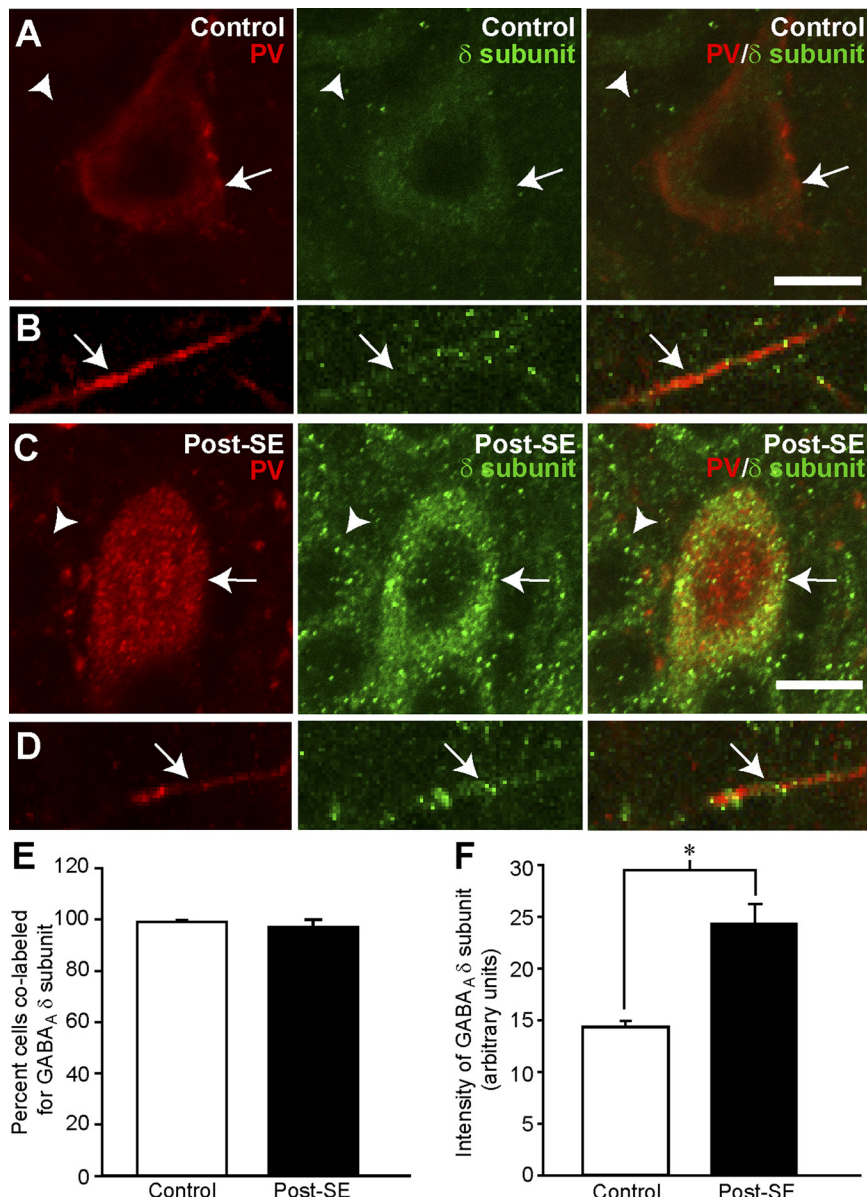


Fig. 2. GABA_A receptor (GABA_AR) δ-subunit expression in parvalbumin (PV) interneurons. *A–D*: confocal images from slices labeled for PV (left) and GABA_AR δ-subunit (center). Merged images (right) show colabeling of PV and GABA_AR δ-subunit in soma (*A*) and a hilar dendrite (*B*) from a control rat and soma (*C*) and a hilar dendrite (*D*) from a post-SE rat. Arrows indicate colabeled cells, and arrowheads point to cells expressing GABA_AR δ-subunit not labeled for PV. Scale bars (10 μ m) in *A* and *C* apply to *A–D*. *E*: summary data show % of PV+ neurons in the hilar-GCL border colabeled for GABA_AR δ-subunit. *F*: histogram of fluorescence intensity for GABA_AR δ-subunit staining in the somata of PV+ neurons from control and post-SE rats.

layer border on the basis of their characteristic morphological and physiological properties. Previous studies have established that dentate PV+ basket cells have axon collaterals largely localized in the granule cell layer, whereas axons of CCK- and somatostatin-expressing interneurons project to the molecular layer (Buckmaster et al. 2002; Hefft and Jonas 2005). Thus the distinctive axonal distribution in the granule cell layer can be used to morphologically identify PV+ interneurons. Apart from morphology, the typical high-frequency, nonadapting firing during depolarizing current injections has been used as a physiological marker of PV+ basket cells (Harney and Jones 2002; Hefft and Jonas 2005; Zhang and Buckmaster 2009). Figure 3*A* illustrates a reconstructed FS-BC with the axon in the granule cell layer. The cell was filled during physiological recordings and processed for post hoc biocytin immunostaining. The FS-BC reconstructed in Fig. 3*A*, *top*, demonstrated characteristic high-frequency, nonadapting firing in response to a 500-pA depolarizing current injection, with low R_{in} and numerous synaptic events during -100 -pA hyperpolarizing

current injection (Fig. 3*A*, *bottom*, and insets in Figs. 4*B* and 5*A*). Additionally, colabeling of the dendrites of the recorded neuron for parvalbumin (Fig. 3*A*, *inset*) confirm the identity of the cell as a PV+ FS-BC. Although our routine immunostaining identified PV labeling in dendrites of biocytin-filled FS-BCs, most FS-BCs did not show somatic labeling for PV. It is likely that the combination of high-chloride internal solution and long-duration recording contributed to the difficulty in detecting somatic PV labeling. Consequently, all FS-BCs in the present study were identified on the basis of a combination of fast-spiking, nonadapting physiology, the presence of axon collaterals in the granule cell layer, and dendritic PV labeling. In addition to FS-BCs, we recorded from non-FS-INs with somata in the hilar-granule cell layer border and axon collaterals distributed in the molecular layer (Fig. 3*B*, *top*). Physiological recordings from the same cell (Fig. 3*B*, *bottom*) illustrate the adapting firing pattern during positive current injection (+200 pA) and the presence of depolarizing sag and high R_{in} in response to negative current injections (-100 pA).

Fig. 3. Morphological and physiological characterization of dentate interneurons projecting to granule cell somata and dendrites. *A, top*: reconstruction of a fast-spiking basket cell (FS-BC) filled during recordings shows the typical morphology with soma and dendrites in blue and axon in GCL in black. ML, molecular layer. *Bottom*: membrane voltage traces from the same cell illustrate the fast-spiking, nonadapting firing pattern during a +500 pA current injection and relatively low membrane hyperpolarization in response to a -100 pA current injection. *Inset*: confocal image of biocytin-filled (BIO) soma and dendrites (arrowheads) of the cell in *A* (*top*) and labeling for PV in the dendrites (*middle*); *bottom*: merged image showing PV colabeling in the biocytin-filled dendrites (arrowheads). Scale bar, 100 μ m. *B, top*: Neurolucida reconstruction of a non-fast-spiking interneuron (non-FS-IN) with axon in the ML. *Bottom*: membrane voltage traces from the same cell show the typical adapting firing during a +200 pA current injection and membrane hyperpolarization and depolarizing sag (arrowhead) during a -100-pA current injection. Note the difference in membrane hyperpolarization in response to -100-pA current injections between the FS-BC (*A*) and non-FS-IN (*B*).

Although the RMPs of FS-BCs and non-FS-INs were not different (RMP in mV: FS-BC -74.0 ± 1.9 in $n = 10$ cells; non-FS-IN -72.3 ± 2.4 in $n = 12$ cells, $P > 0.05$ by Student's *t*-test), the frequency of FS-BC firing in response to a +800-pA current injection was significantly greater (frequency in Hz: FS-BC 112.1 ± 7.9 in $n = 12$ cells; non-FS-IN 52.0 ± 5.7 in $n = 8$ cells, $P < 0.05$ by Student's *t*-test) and the R_{in} lower (R_{in}

in MΩ: FS-BC 93.0 ± 10.6 in $n = 12$ cells; non-FS-IN 233.3 ± 6.8 in $n = 8$ cells, $P < 0.05$ by Student's *t*-test) than in non-FS-IN. Together, these morphological and physiological characteristics are consistent with earlier studies (Harney and Jones 2002) and were used to reliably distinguish FS-BCs from a potentially diverse set of non-FS-INs projecting to the molecular layer.

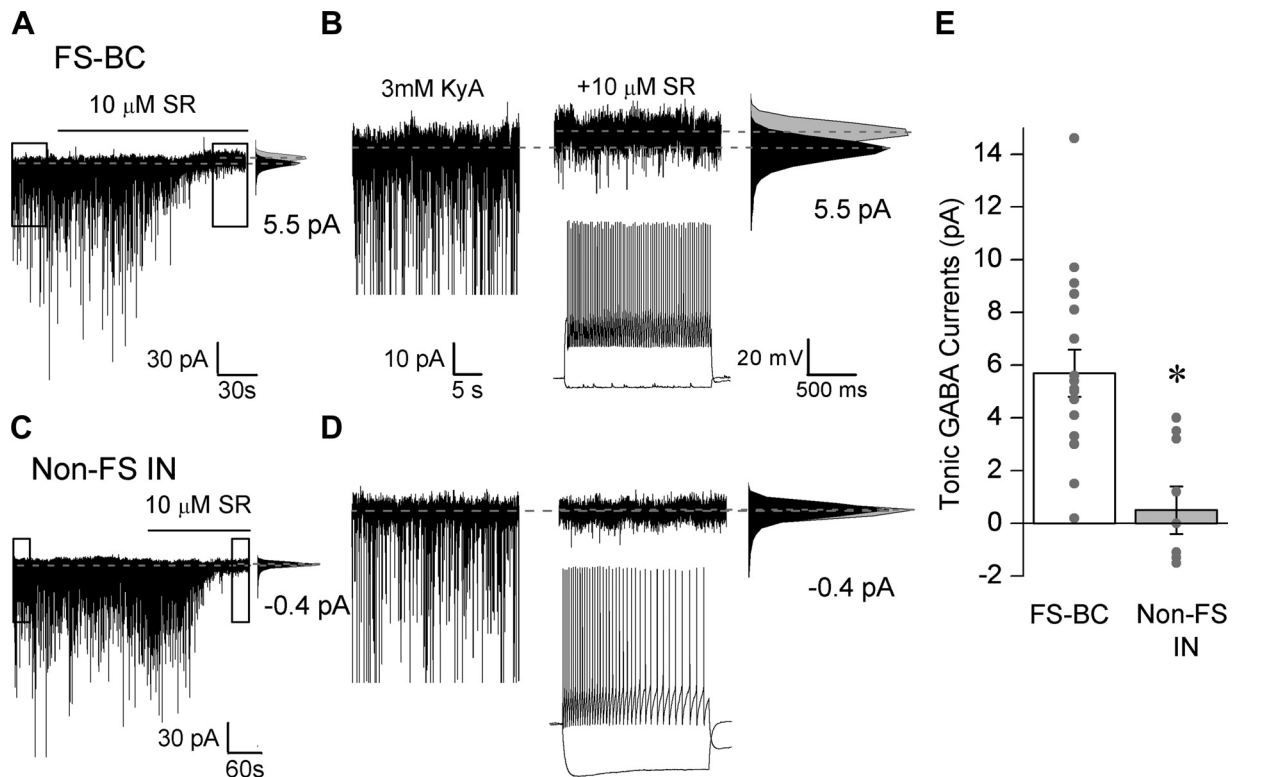
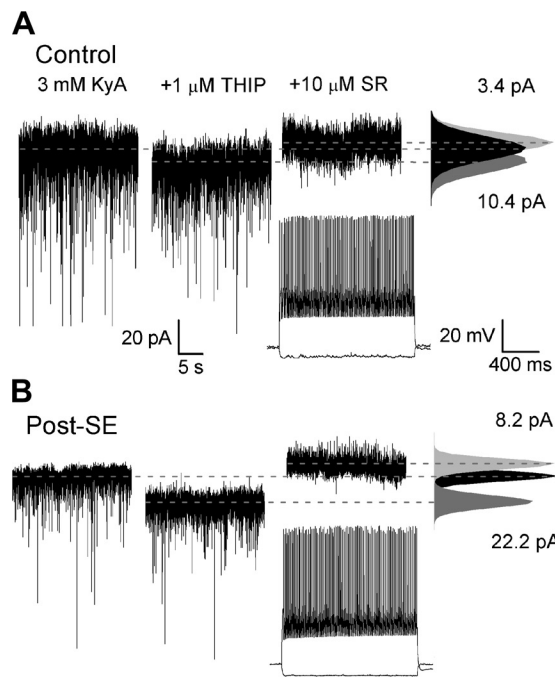


Fig. 4. Expression of tonic GABA currents (I_{GABA}) in dentate FS-BCs. *A*: representative voltage-clamp recordings ($V_{hold} = -70$ mV) from a FS-BC in the hilar-GCL border illustrates the presence of tonic I_{GABA} blocked by SR95531 (gabazine, 10 μ M). *B*: expanded 30-s traces of the boxed area in *A*. Gaussian fits to all-points histograms derived from the illustrated recording periods in control conditions, in the presence of 3 mM kynurenic acid (KyA), and after the addition of gabazine used to determine tonic current amplitude are shown on right. Dashed lines indicate Gaussian means, and the difference currents are noted. *Inset*: membrane voltage trace from the same cell shows fast-spiking firing. *C*: representative voltage-clamp recordings ($V_{hold} = -70$ mV) from a non-FS-IN in the hilar-GCL border illustrates lack of tonic I_{GABA} on blocking GABA_AR with SR95531 (10 μ M). *D*: expanded 30-s traces of the boxed area in *C*. Gaussian fits to all-points histograms used to determine tonic current amplitude are presented on right. *Inset*: membrane voltage trace from the cell in *C* and *D* shows adapting firing. *E*: summary data of tonic I_{GABA} amplitude in 3 mM kynurenic acid in FS-BCs and non-FS-IN. Individual data points are represented by gray dots. * $P < 0.05$ by unpaired Student's *t*-test.

We examined interneurons in the hilar-granule cell layer border for the presence of tonic I_{GABA} . Recordings were performed in the presence of the glutamate receptor antagonist KyA (3 mM), and tonic I_{GABA} was measured as the baseline current blocked by the GABA_AR antagonist SR95531 (gabazine, 10 μ M). Recordings were obtained at physiological temperature and in the absence of added GABA or GABA transporter inhibitors. As illustrated by representative recordings from an FS-BC in Fig. 4A and the magnified 30-s segments of the boxed areas in Fig. 4A (Fig. 4B), SR95531 caused a small but significant shift in the baseline current, indicating the presence of tonic I_{GABA} in FS-BCs ($P < 0.05$, paired Student's t -test). In contrast, non-FS-INs lacked tonic I_{GABA} and showed little shift in baseline after addition of SR95531 (Fig. 4, C and D; $P > 0.05$, paired Student's t -test). On average the magnitude of tonic I_{GABA} in morphologically and physiologically identified FS-BCs was significantly greater than in non-FS-INs (Fig. 4E; tonic I_{GABA} in pA: FS-BC 5.7 ± 0.9 , $n = 17$; non-FS-IN: 0.5 ± 0.9 , $n = 9$; $P < 0.05$ by Student's t -test). Thus, consistent with the anatomical data showing colabeling of GABA_AR δ -subunits with PV+ interneurons (Fig. 2), our physiological data demonstrate that dentate FS-BCs express tonic I_{GABA} . Additionally, the results demonstrate that the magnitude of tonic I_{GABA} in FS-BCs is greater than in non-FS-INs.

Status epilepticus enhances FS-BC tonic I_{GABA} . Since our immunostaining data (Fig. 2) indicate that the expression of GABA_AR δ -subunits in PV+ interneurons is enhanced 1 wk after SE, we examined whether FS-BC tonic I_{GABA} are increased after SE. In recordings from FS-BCs in control rats, THIP (1 μ M), a preferential agonist of GABA_ARs containing δ -subunits (Brown et al. 2002), enhanced tonic I_{GABA} , confirming the contribution of GABA_AR δ -subunits (Fig. 5, A and C; tonic I_{GABA} in pA: 5.3 ± 2.0 in KyA and 11.5 ± 2.7 in THIP, $n = 7$ cells, $P < 0.05$, paired Student's t -test). Similarly, THIP enhanced tonic I_{GABA} in FS-BCs from post-SE rats (Fig. 5, B and C; tonic I_{GABA} in pA: 14.0 ± 2.1 in KyA and 21.9 ± 2.1 in THIP, $n = 7$ cells, $P < 0.05$, paired Student's t -test). Importantly, the magnitude of FS-BC tonic I_{GABA} , both in



KyA and in THIP, was significantly greater in post-SE rats compared with control rats (Fig. 5, A-C; $P < 0.05$, t -test). Application of THIP (1 μ M) caused a significantly greater increase in baseline currents in FS-BCs from post-SE rats (baseline current increase in THIP in pA: control FS-BCs: 6.0 ± 1.4 , $n = 8$ cells; post-SE FS-BCs 10.8 ± 1.6 , $n = 10$ cells, $P < 0.05$ by Student's t -test), confirming that increases in membrane expression of GABA_AR δ -subunits contribute to post-SE increase in FS-BC tonic I_{GABA} . To eliminate the possibility that THIP, like GABA, may alter GABA_AR antagonist binding (Bianchi and Macdonald 2001) and confound estimation of tonic I_{GABA} , we also measured tonic I_{GABA} in control aCSF in the presence of KyA and without perfusion of THIP. When normalized to cell membrane capacitance, to eliminate confounding effects due to differences in cell size, tonic I_{GABA} in FS-BCs from post-SE rats was greater than those from control rats (Fig. 5D; tonic I_{GABA} current density in pA/pF: control 0.10 ± 0.02 , $n = 11$ cells; post-SE 0.23 ± 0.05 , $n = 7$ cells, $P < 0.05$, Student's t -test). Moreover, FS-BC tonic I_{GABA} measured in the presence of the GABA transporter antagonist NO-711 (10 μ M), to abolish potential post-SE differences in GABA transporter function, was also enhanced after SE (Fig. 5E; tonic I_{GABA} in pA: control 14.7 ± 2.6 , $n = 6$ cells; post-SE 24.6 ± 3.1 , $n = 6$ cells, $P < 0.05$, Student's t -test). Comparison of the intrinsic properties measured during whole cell recordings revealed no change in either R_{in} or RMP between FS-BCs from control and post-SE rats (R_{in} in MΩ: control 93.0 ± 10.6 , $n = 12$ cells; post-SE 97.6 ± 11.2 , $n = 9$ cells, $P > 0.05$, Student's t -test; RMP in mV: control -74.0 ± 1.9 , $n = 10$ cells; post-SE -75.0 ± 2.4 , $n = 10$ cells, $P > 0.05$, Student's t -test). R_{in} was measured in response to a -100-pA current injection. Our measurements of FS-BC tonic I_{GABA} demonstrate, unequivocally, that tonic I_{GABA} is present in FS-BCs and is enhanced after SE. Our results indicate that SE-induced increases in the expression of GABA_ARs with δ -subunits likely contribute to increases in FS-BC tonic I_{GABA} after SE.

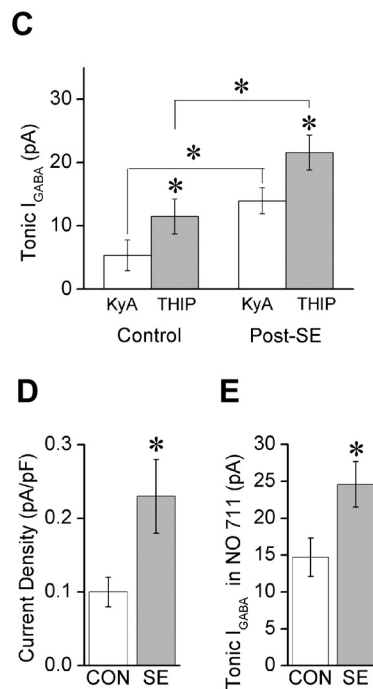


Fig. 5. Tonic I_{GABA} in dentate FS-BCs are enhanced after SE. A and B: segments (30 s) of representative voltage-clamp recordings ($V_{hold} = -70$ mV) from control (A) and post-SE (B) FS-BCs illustrate the enhancement of tonic I_{GABA} by addition of 4,5,6,7-tetrahydroisoazolo[5,4-c]pyridin-3-ol (THIP, 1 μ M). Tonic I_{GABA} was measured as the current blocked by SR95531 (10 μ M). Panels on right show Gaussian fits to all-points histograms of the 30-s recording periods in 3 mM kynurenic acid, after the addition of THIP (1 μ M), and in SR95531. Dashed lines indicate Gaussian means, and the difference currents are noted. Insets: membrane voltage traces show fast-spiking firing of the respective cells. C: summary of the magnitude of FS-BC tonic I_{GABA} in 3 mM kynurenic acid and after perfusion of THIP (1 μ M) in controls and after SE. D: histogram presents baseline tonic I_{GABA} recorded in 3 mM kynurenic acid normalized to the cell membrane capacitance. E: tonic I_{GABA} in control and post-SE FS-BCs measured with the GABA transporter antagonist NO-711 (10 μ M) in the presence of 3 mM kynurenic acid. * $P < 0.05$ by paired and unpaired Student's t -test.

Spillover of synaptically released GABA into the extrasynaptic space is known to contribute to tonic I_{GABA} (Glykys and Mody 2007). Therefore, one possibility is that the post-SE enhancement of tonic I_{GABA} reflects post-SE increases in synaptic GABA release. Previous studies have demonstrated that in granule cells the frequency of sIPSCs is decreased after SE (Kobayashi and Buckmaster 2003), discounting the possible contribution of enhanced GABA spillover from inhibitory synapses to granule cells. To examine whether increases in synaptic GABA release to FS-BCs could contribute to the observed enhancement of tonic I_{GABA} after SE, we analyzed the frequency of sIPSCs in cells examined for changes in tonic I_{GABA} (in Fig. 5). As illustrated by representative traces (Fig. 6, A and B), there was a considerable decrease in the frequency of sIPSCs in FS-BCs from post-SE rats (Fig. 6B; sIPSC frequency in Hz: control median = 7.0, IQR = 3.7–13.7, mean \pm SE = 10.9 \pm 0.5, n = 10 cells; post-SE median = 5.0, IQR = 2.6–10.6, mean \pm SE = 8.9 \pm 0.6, n = 7 cells, P < 0.05, K-S test). Additionally, FS-BC sIPSC amplitude was reduced (in pA: control median = 17.7, IQR = 10.6–34.2, mean \pm SE = 30.3 \pm 1.6, n = 10 cells; post-SE median = 14.7, IQR = 8.4–26.2, mean \pm SE = 22.5 \pm 1.1, n = 7 cells, P < 0.05, K-S test) and decay increased (in ms: control median = 3.65, IQR = 2.9–6.1, mean \pm SE = 5.4 \pm 0.2, n = 10 cells; post-SE median = 4.8, IQR = 3.3–8.5, mean \pm SE = 6.3 \pm 0.3, n = 7 cells, P < 0.05, K-S test) after SE. However, sIPSC charge transfer showed a small but statistically significant decrease after SE (Fig. 6C; charge transfer in pA·ms: control median = 83.66, IQR = 52.3–150.2, mean \pm SE = 133.24 \pm 6.1, n = 10 cells; post-SE median = 75.5, IQR = 48.2–140.8, mean \pm SE = 111.138 \pm 4.7, n = 7 cells, P < 0.05, K-S test). Additionally, THIP (1 μ M) caused a small but statistically significant decrease in sIPSC amplitude in both control and post-SE FS-BCs (in pA: control median = 17.7, IQR = 10.6–34.2, mean \pm SE = 30.3 \pm 1.6, n = 10 cells; THIP median = 15.5, IQR = 8.9–28.8, mean \pm SE = 26.1 \pm 1.2, n = 10 cells, P < 0.05, K-S test; post-SE median = 14.7, IQR = 8.4–26.2, mean \pm SE = 22.5 \pm 1.1; THIP median =

14.1, IQR = 7.6–23.05, mean \pm SE = 17.9 \pm 0.7, n = 7 cells, P < 0.05, K-S test). Together, the reductions in both FS-BC and granule cell sIPSC frequency after SE argue against the possibility that synaptic spillover underlies post-SE increase in tonic I_{GABA} .

Depolarizing shift in FS-BC E_{GABA} after status epilepticus. The ability of GABA_AR activation to inhibit neuronal excitability depends on a combination of hyperpolarization, when E_{GABA} is negative to neuronal RMP (hyperpolarizing driving force), and shunting inhibition resulting from GABA_AR conductance. E_{GABA} depends on the electrochemical gradients for Cl⁻ and, to a lesser extent, HCO₃⁻ ions and can be positive to neuronal RMP during development when intracellular chloride is relatively high (Ben-Ari 2001). Developmental changes in chloride transporters are instrumental in maintaining a hyperpolarizing E_{GABA} in adult neurons (Rivera et al. 2005). However, there may be cell type-specific differences in chloride regulation (Banke and McBain 2006). Remarkably, pilocarpine-induced SE contributes to a depolarizing shift in dentate granule cell E_{GABA} 1 wk after SE (Pathak et al. 2007). Since the net effect of the observed increase in FS-BC tonic I_{GABA} on FS-BC and dentate excitability is likely to depend on whether E_{GABA} is positive or negative to the RMP, we examined whether FS-BC RMP and E_{GABA} are altered after SE.

To avoid perturbations of the intracellular chloride concentration, we used gramicidin-perforated-patch recordings (Bil-lups and Attwell 2002; Pathak et al. 2007) and measured the RMP and reversal potential of GABA-evoked currents in parallel within the same FS-BC. Upon establishment of adequate access (see MATERIALS AND METHODS), we first determined the neuronal firing pattern in response to depolarizing current injections before perfusion of TTX (1 μ M) to block action potential generation. Next, in the absence of added GABA, we recorded FS-BCs current responses to -130 to $+10$ mV voltage ramps from a holding potential of -60 mV (Fig. 7A). The potential at which the holding current was 0 pA was measured as the RMP (Fig. 7A). In interleaved recordings preformed at 40-s intervals, voltage ramps were repeated

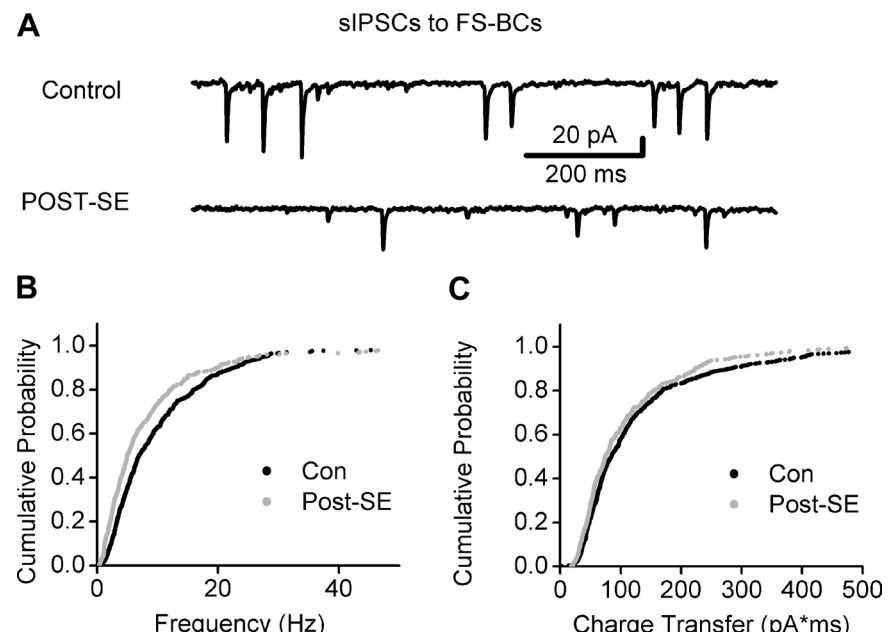


Fig. 6. Decrease in FS-BC spontaneous inhibitory postsynaptic current (sIPSC) frequency after SE. A: representative traces of voltage-clamp recordings from control (top) and post-SE (bottom) FS-BCs show the higher sIPSC frequency in the control FS-BC. Note the decrease in sIPSC frequency in the recording from the post-SE FS-BC. B and C: cumulative probability plot of the sIPSC instantaneous frequency (B) and charge transfer (C) in control and post-SE FS-BCs measured with symmetrical chloride from a holding potential of -70 mV in kynurenic acid (3 mM). The same number of individual events was selected from each cell to develop the cumulative probability distribution (control: n = 10 cells; post-SE: n = 7 cells).

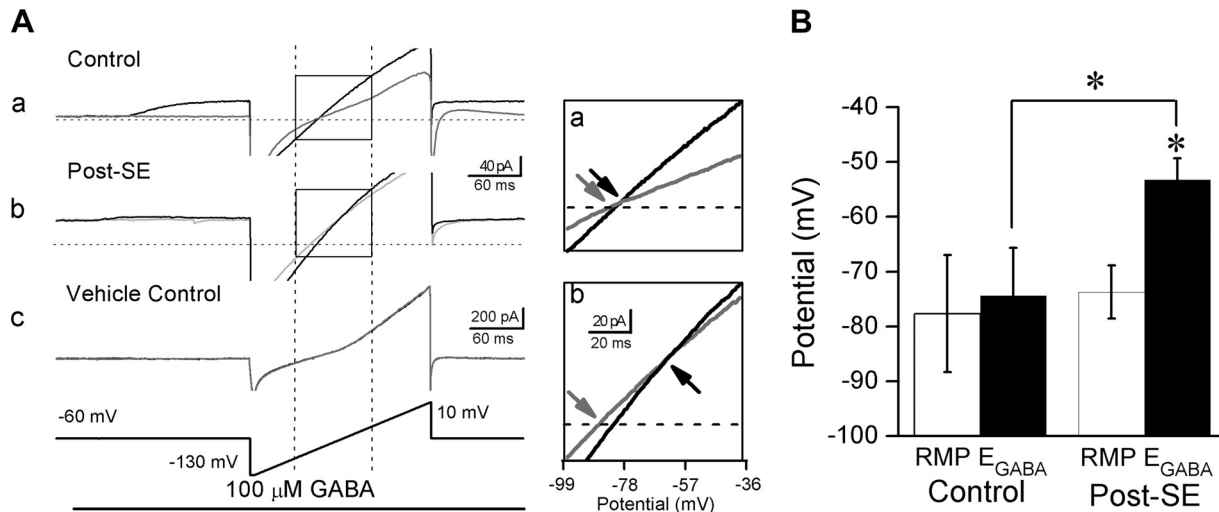


Fig. 7. FS-BC GABA reversal potential (E_{GABA}) is depolarized after status epilepticus. **A:** gramicidin-perforated-patch recordings show current traces from control (*a*) and post-SE (*b*) FS-BCs recorded during depolarizing ramps (bottom) in the absence of GABA (gray) and during pressure application of 100 μ M GABA (black). Horizontal dashed line represents holding current (I_{hold}) = 0 pA at which resting membrane potential (RMP) was determined (gray arrows in insets). The ramp potential at which the current traces without GABA and with GABA crossed represents E_{GABA} (black arrow in inset). Vertical dashed lines intersecting the command potential schematic show the range of command voltage in the boxed area. **Insets:** expanded traces of boxed regions illustrate the FS-BC RMP (gray arrow) and E_{GABA} (black arrow) in control (*a*) and post-SE (*b*) FS-BCs. *c:* Representative traces from a control experiment showing overlapping current traces in response to depolarizing ramps in the absence of (gray) and during pressure application of the vehicle (black). **B:** summary plot of FS-BC RMP and E_{GABA} . * $P < 0.05$ by paired and unpaired Student's *t*-test.

during local pressure application of GABA (100 μ M). The potential at which the currents generated during the voltage ramp in the absence and the presence of GABA crossed was measured as E_{GABA} . As shown in Fig. 7*Aa*, *inset*, RMP in control FS-BCs was not different from the potential at which the current traces obtained in the presence and absence of GABA crossed (in mV: $E_{GABA} = -74.2 \pm 8.8$, RMP -77.6 ± 10.7 , in $n = 6$ cells, $P > 0.05$ by paired Student's *t*-test). These data suggest that GABA_AR activation likely contributes to shunting inhibition in control FS-BCs. In control experiments, we found no difference between E_{GABA} measured with voltage ramp and voltage step protocols in the same cell (in mV: E_{GABA} with voltage ramp -77.28 ± 2.89 , E_{GABA} with voltage step -80.0 ± 3.68 , in $n = 4$ cells, $P > 0.05$ by paired Student's *t*-test), indicating that the voltage ramp protocol can be used to reliably estimate E_{GABA} . In contrast to control rats, E_{GABA} measured in FS-BCs from post-SE rats was significantly more depolarized than RMP (Fig. 7*Ab*; in mV: $E_{GABA} = -53.3 \pm 4.0$, RMP -73.7 ± 4.9 in $n = 7$ cells, $P < 0.05$ by paired Student's *t*-test). Overlapping interleaved traces from control experiments performed under identical conditions in the absence and during pressure application of vehicle without GABA confirmed the absence of pressure artifacts under our recording conditions (Fig. 7*Ac*). While the difference in RMP between control and post-SE FS-BCs was not statistically significant (Fig. 7*B*; FS-BC RMP in mV: control -77.6 ± 10.7 , $n = 6$; post-SE -73.7 ± 4.9 , $n = 7$, $P > 0.05$ by Student's *t*-test), there was a clear depolarizing shift in FS-BC E_{GABA} after SE (Fig. 7*B*; FS-BC E_{GABA} in mV: control -74.2 ± 8.8 , $n = 6$; post-SE -53.3 ± 4.0 , $n = 7$, $P < 0.05$ by Student's *t*-test).

We directly tested whether activation of GABA receptors leads to membrane depolarization in FS-BCs from post-SE rats. Although cell-attached recordings from FS-BCs showed spontaneous firing when external potassium was elevated to 3 mM and above (not shown), as observed by Fricker et al. (1999), few interneurons fired spontaneously under our recording conditions

with 2.5 mM external potassium. To avoid confounding effects due to changes in RMP, cell-attached recordings from FS-BCs were obtained in standard aCSF containing 2.5 mM potassium. Cell-attached recordings showed that while pressure application of the GABA_AR agonist muscimol (50 μ M) caused little change in membrane potential in control FS-BCs, it consistently depolarized FS-BCs from post-SE rats (Fig. 8; maximum membrane potential change in muscimol in mV: control 0.3 ± 1.3 , $n = 5$; post-SE 7.6 ± 2.1 , $n = 8$, $P < 0.05$ by Student's *t*-test). Together, comparison of RMP and E_{GABA} in FS-BCs from control and post-SE rats under identical experimental conditions suggests that activation of extrasynaptic GABA_ARs may be shunting under control conditions and result in depolarizing currents after SE.

Previous studies have identified that FS-BC synaptic E_{GABA} undergoes a developmental hyperpolarizing shift and have suggested that increases in the expression of the potassium-chloride cotransporter KCC2 (Sauer and Bartos 2010) may underlie this effect. Since changes in expression of KCC2 have been shown to contribute to post-SE alterations in granule cell E_{GABA} (Pathak et al. 2007), we examined FS-BCs for post-SE changes in KCC2 expression. Examination of sections immunostained for PV and KCC2 revealed the presence of KCC2 localized to the periphery of PV+ profiles in both control and post-SE rats (Fig. 9). Quantification of the fluorescence intensity for KCC2 subunit expression in PV+ neurons identified a significant post-SE decrease in KCC2 along the margins of PV+ profiles in the hilar-granule cell layer border (grayscale intensity in arbitrary units: control 15.7 ± 2.6 , $n = 29$ cells from 15 sections in 3 rats; post-SE 9.8 ± 1.1 , $n = 36$ cells from 15 sections in 3 rats, $P < 0.05$ by Student's *t*-test). The observed decrease in KCC2 expression in PV+ neurons likely contributes to the depolarizing shift in FS-BC E_{GABA} after SE.

Impact of tonic g_{GABA} and E_{GABA} on FS-BC excitability: isolated basket cell simulations. How do the presence and post-SE changes in tonic g_{GABA} , together with the depolarized E_{GABA} , modify FS-BC excitability? Given the concurrent changes in

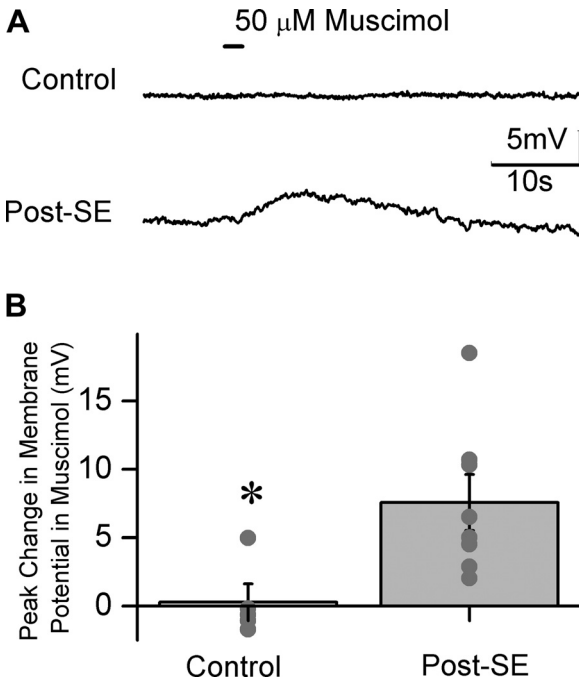


Fig. 8. GABA agonists depolarize FS-BCs 1 wk after SE. *A*: cell-attached recordings show membrane voltage traces from control (*top*) and post-SE (*bottom*) FS-BC recorded during pressure application of 50 μ M muscimol (black bar). *B*: summary plot of the maximum change in FS-BC membrane potential in response to muscimol application. Individual data points are represented by gray dots. * P < 0.05 by unpaired Student's *t*-test.

conductance and reversal of tonic I_{GABA} , and potential confounding SE-induced changes in the intrinsic physiology of FS-BCs (unpublished observations) that are as yet unknown, it is difficult to isolate how alterations in FS-BC tonic I_{GABA} , both singly and when coupled with depolarized E_{GABA} , modify network activity in biological experiments. Therefore, we adopted computational modeling to determine how systematic changes in FS-BC tonic g_{GABA} , in the presence and absence of the observed depolarizing shift in GABA reversal, influence FS-BC and dentate network excitability. A recent study conducted with generic single compartmental models showed that when E_{GABA} is depolarizing, tonic g_{GABA} increases neuronal excitability only in a narrow range of g_{GABA} . With additional increases in tonic g_{GABA} , the shunting effect of the conductance overwhelms the depolarizing currents, resulting in net inhibition (Song et al. 2011). To systematically examine how post-SE changes in tonic g_{GABA} and E_{GABA} influence FS-BC excitability, we implemented biophysically realistic multicompartmental simulations of FS-BCs (Santhakumar et al. 2005). As illustrated in Fig. 10*A*, the model FS-BC fired at a frequency of 100 Hz in response to a 800-pA current injection, simulating the experimentally determined characteristic high-frequency firing and low R_{in} of biological dentate FS-BCs (for detailed comparison of the active and passive properties of the model FS-BC and biological basket cells see Table 3 in Santhakumar et al. 2005). To determine the magnitude of tonic g_{GABA} that generates the biologically observed tonic I_{GABA} , we simulated voltage-clamp recordings in model FS-BCs and examined how increases in tonic g_{GABA} influence the magnitude of tonic I_{GABA} and R_{in} . Systematically increasing tonic g_{GABA} from 5 nS/cm² resulted in negligible tonic I_{GABA} and no change in R_{in} in the model FS-BC up to a conductance of 0.5 μ S/cm². Tonic g_{GABA} of 1 μ S/cm² resulted in 10-pA tonic I_{GABA} , comparable to exper-

imentally observed tonic I_{GABA} with g_{GABA} contributing to <0.5% of the model FS-BC resting conductance. Increasing tonic g_{GABA} to 10 μ S/cm² resulted in 60-pA tonic I_{GABA} , a 3.3-M Ω decrease in R_{in} (Fig. 10*B*), and a 2.7% decrease in FS-BC membrane conductance. When tonic g_{GABA} was increased to 50 μ S/cm² and above, tonic I_{GABA} was >250 pA and R_{in} decreased by >10 M Ω , which is well outside the range observed in our experimental data (Fig. 5). The effect of tonic g_{GABA} on tonic I_{GABA} and R_{in} in model FS-BCs was unchanged even when the g_{GABA} was restricted to the soma and proximal dendritic compartments (Fig. 10*B*). Since our experimental estimation of ~5-pA tonic I_{GABA} in control FS-BCs is 1) without added GABA, 2) in continuously perfused slices, and 3) at physiological temperature, it is likely an underestimation. Note also that in the presence of the GABA transporter antagonist tonic I_{GABA} in FS-BCs is >10 pA, despite the presumably low activity levels in slices perfused with glutamate receptor antagonists (Fig. 5*E*). Therefore, we expect that tonic g_{GABA} between 1 and 10 μ S/cm² (corresponding to 10- to 60-pA tonic I_{GABA}) in our simulations represents the range of biologically realistic tonic I_{GABA} levels during neuronal activity.

Next, we examined the effect of tonic I_{GABA} on the excitability of model FS-BCs during excitatory synaptic inputs. Model FS-BCs received 200-Hz Poisson-distributed excitatory inputs to their distal dendrites, to simulate perforant path AMPA-mediated synaptic inputs. The rise and decay of the AMPA synapse was constrained by experimental data as described previously (Santhakumar et al. 2005). g_{AMPA} was set either at 3 nS to simulate low excitatory inputs that lead to minimal FS-BC firing (Fig. 10, *C* and *D*) or at 20 nS, which resulted in model FS-BC firing at >30 Hz in the absence of tonic g_{GABA} (Fig. 10*E*). Model FS-BCs received identical input trains in each simulation. In the first set of simulations, the reversal potential for the tonic g_{GABA} was set to -74 mV, the experimentally determined E_{GABA} in control FS-BCs. Tonic g_{GABA} was simulated as a uniformly distributed leak conductance in the range of 5 nS/cm² to 5 mS/cm². This wide range of tonic g_{GABA} encompassed the biologically relevant range of 1–10 μ S/cm², and extended to include conductance values that resulted in biphasic changes in neuronal excitability similar to those described in previous studies (Song et al. 2011). Tonic g_{GABA} in the range of 1 μ S/cm² to 1 mS/cm² decreased model FS-BC firing during both low (3 nS)- and high (20 nS)-conductance excitatory inputs and abolished firing at g_{GABA} over 75 μ S/cm² and 0.3 mS/cm², respectively (Fig. 10, *C*–*E*). Since RMP of the model FS-BC was -70 mV, the decrease in excitability when E_{GABA} was -74 mV is consistent with shunting inhibition. When E_{GABA} was set to -54 mV, the experimentally determined E_{GABA} in post-SE FS-BCs, increasing tonic g_{GABA} led to an initial increase in model FS-BC firing when tonic g_{GABA} was over 1 μ S/cm², which reached a maximum when tonic g_{GABA} was 1 mS/cm². FS-BC firing declined with further increase in tonic g_{GABA} and was eventually completely suppressed (Fig. 10, *C*–*E*). Model FS-BC firing during excitatory synaptic inputs delivered in the presence of depolarizing E_{GABA} (-54 mV) and 1 μ S/cm² to 1 mS/cm² tonic g_{GABA} increased even though E_{GABA} was more hyperpolarized than the model FS-BC action potential threshold (-40.5 mV). The simulation results are consistent with recent studies demonstrating that, in the presence of a depolarizing E_{GABA} , progressively increasing tonic g_{GABA} leads to an initial neuronal depolarization followed by shunting inhibition with

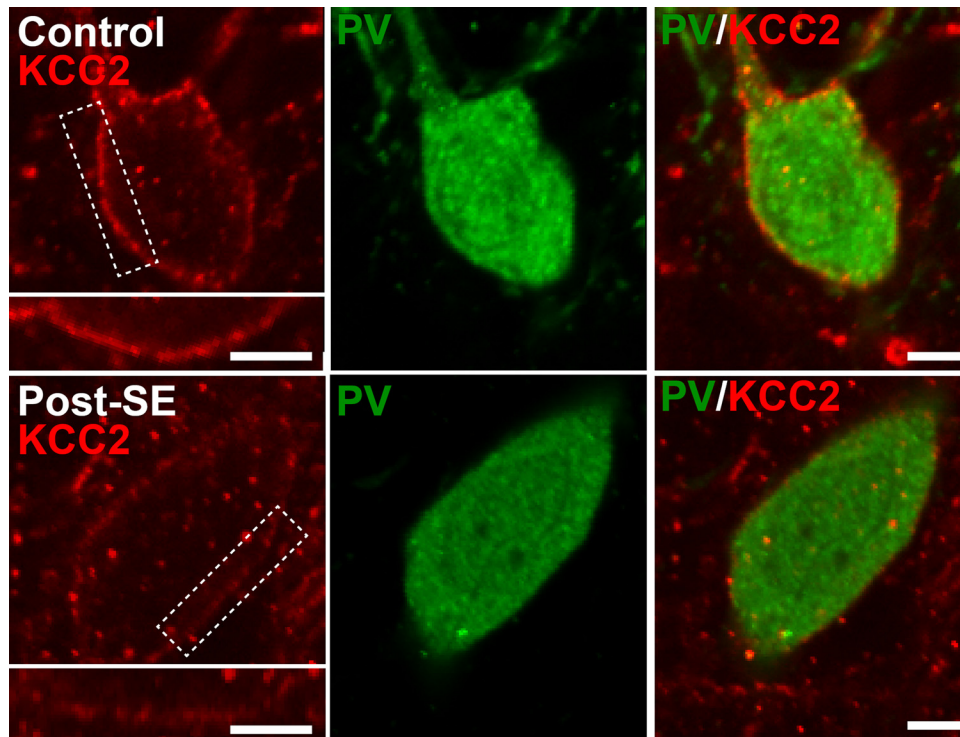


Fig. 9. SE decreases expression of KCC2 in PV interneurons. Confocal images from sections labeled for KCC2 (*left*) and PV (*center*) are shown. Merged images (*right*) show colabeling of KCC2 particularly in the periphery of the PV-positive neurons from a control (*top*) and a post-SE (*bottom*) rat. Boxed areas are shown at higher magnification in *insets*. Images were obtained with identical camera settings. Scale bars, 10 μ m.

further increases (Song et al. 2011). However, our simulations demonstrate that in the biologically relevant range of 1–10 μ S/cm² tonic g_{GABA} , the experimentally observed post-SE E_{GABA} (-54 mV) reverses the decrease in excitability mediated by tonic I_{GABA} .

In additional simulations, we restricted tonic g_{GABA} to the somatic and proximal dendritic compartments to examine whether dendritic tonic g_{GABA} influenced neuronal excitability by local modulation of synaptic inputs. In simulations performed without tonic g_{GABA} in the distal dendritic compartments where the excitatory synapses were located, both the range of tonic g_{GABA} values that modulated model FS-BC excitability and the biphasic nature of the changes were indistinguishable from simulations that included tonic g_{GABA} in all compartments (not shown). These simulations results suggest that local dendritic modulation of synaptic inputs does not underlie the effect of tonic g_{GABA} on model FS-BC excitability. Thus the isolated FS-BC simulations predict that post-SE increases in tonic g_{GABA} in the biologically relevant range would, in the absence of concomitant changes in E_{GABA} (at $E_{GABA} = -74$ mV), decrease FS-BC excitability during both low and moderate excitatory synaptic drive (Fig. 10C, *left*, and Fig. 10, *D* and *E*). Alternatively, a depolarizing shift in E_{GABA} , when not accompanied by changes in tonic g_{GABA} , would enhance FS-BC excitability (Fig. 10C, compare *left* and *right* at each tonic g_{GABA} ; Fig. 10, *D* and *E*, compare firing at identical tonic g_{GABA} levels). However, the combined effect of the concurrent increase in tonic g_{GABA} and depolarized E_{GABA} is to maintain the control levels of FS-BC excitability during low levels of excitatory synaptic drive (Fig. 10D).

Effect of seizure-induced FS-BC GABAergic plasticity on dentate excitability: dentate network simulations. Our experimental data have demonstrated two distinct SE-induced changes in the inhibitory tone of dentate FS-BCs, namely, an increase in tonic I_{GABA} and a positive shift in the driving force

for I_{GABA} after SE. Since both tonic I_{GABA} and E_{GABA} are also altered in granule cells after SE (Pathak et al. 2007; Zhan and Nadler 2009; Zhang et al. 2007), we adopted computational simulations to determine how seizure-induced plasticity in FS-BCs tonic inhibition affects dentate network excitability independent of, and in the absence of, other confounding changes. First, we examined whether the post-SE changes in FS-BC E_{GABA} altered dentate excitability in the absence of tonic g_{GABA} . The 1,000+ dentate neuronal network based on Santhakumar et al. (2005) was simulated as a ring and included 20% sprouting (see MATERIALS AND METHODS). The network included two major interneuronal populations, FS-BCs and hilar dendritically projecting HIPP cells. Since simulating post-SE hilar neuronal loss by removing HIPP cells from the network would disproportionately enhance the role of FS-BCs, the first set of simulations were performed without introducing hilar neuronal loss. Networks received 2.5-Hz spontaneous activity for the entire duration of the simulation. A single synchronous input to 100 adjacent granule cells was used to simulate focal perforant path-evoked network activity. In the absence of tonic g_{GABA} , changing model FS-BC E_{GABA} (of inhibitory synaptic inputs to model FS-BCs from other FS-BCs and hilar interneurons) from -74 mV to -54 mV did not change either the spontaneous background activity level or average granule cell firing in response to synchronous activation (Fig. 11, *A₁* and *B₁*). This is consistent with the ability of the inhibitory synaptic conductance to provide shunting inhibition even when E_{GABA} is more depolarized than RMP (Song et al. 2011; Vida et al. 2006).

Next, we introduced tonic g_{GABA} with activity-dependent synaptic spillover conductance (see MATERIALS AND METHODS) in model FS-BCs. In one group of simulations, E_{GABA} for both tonic and synaptic g_{GABA} was set to -74 mV as observed in controls. Tonic I_{GABA} was increased between 3 μ S/cm², contributing to 18-pA tonic I_{GABA} similar to levels observed in

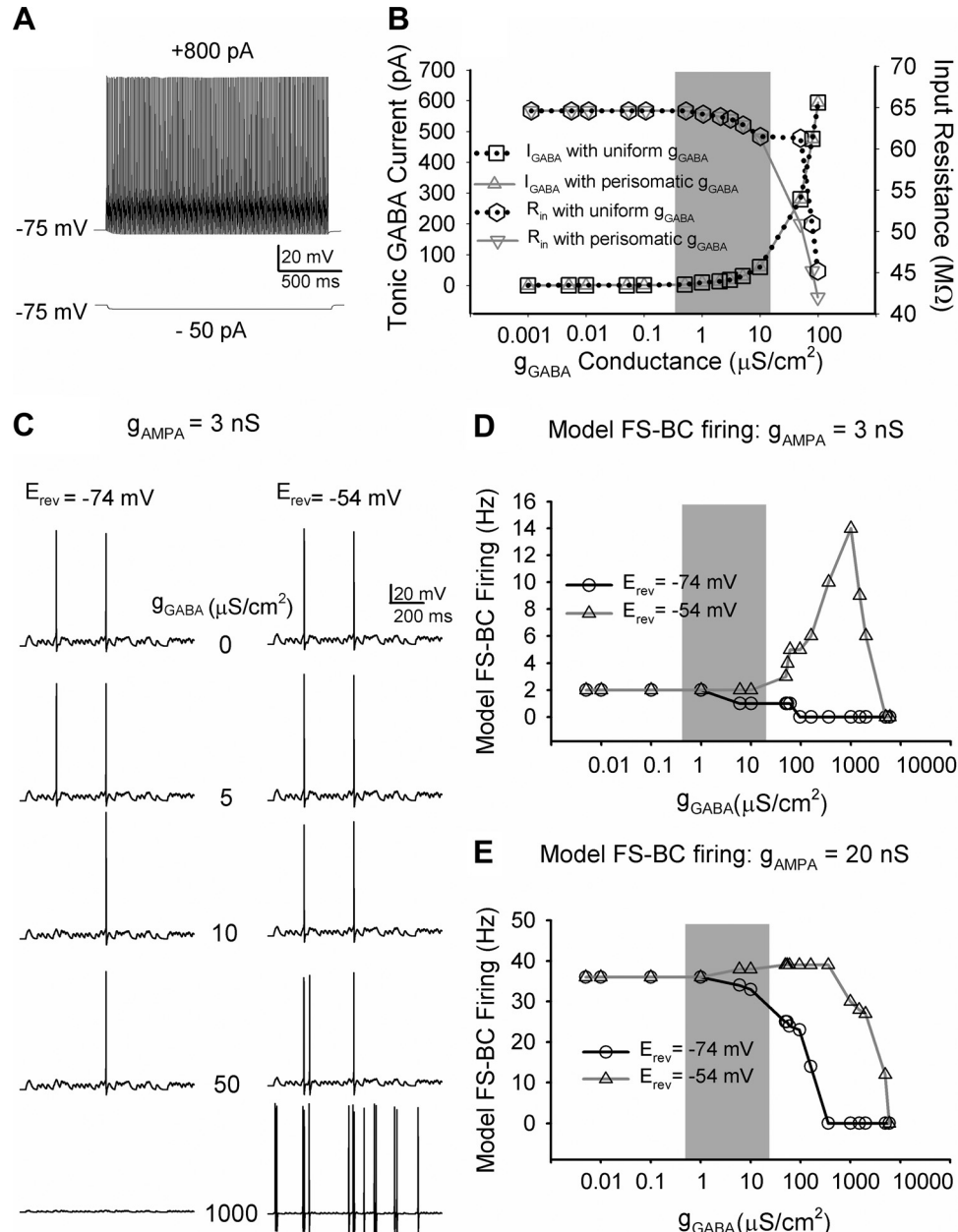


Fig. 10. Effect of GABA reversal and tonic GABA conductance (g_{GABA}) on model FS-BC excitability. **A:** responses of biophysically realistic multicompartmental model FS-BC to depolarizing and hyperpolarizing current injections illustrate nonadapting firing and low input resistance (R_{in}). **B:** summary plot shows tonic I_{GABA} and R_{in} in model FS-BCs as a function of tonic g_{GABA} . In simulations with perisomatic g_{GABA} , tonic GABA channels were distributed only in the soma and proximal dendrite. Simulations incorporated voltage-clamp recording conditions with symmetrical chloride and $V_{\text{hold}} = -70 \text{ mV}$. Shaded region represents biologically relevant tonic I_{GABA} and g_{GABA} range. **C:** membrane voltage traces illustrate firing in FS-BC simulations during 200 Hz during identical Poisson-distributed excitatory inputs when tonic g_{GABA} is systematically increased from 0 to $1 \text{ mS}/\text{cm}^2$. Peak amplitude of input synaptic conductance (g_{AMPA}) was 3 nS . Simulations were performed with control (-74 mV , left) and post-SE (-54 mV , right) E_{GABA} values (E_{rev}). **D:** summary plot of FS-BC firing evoked by 200-Hz excitatory synaptic inputs (3 nS peak conductance) in the presence of increasing tonic g_{GABA} in FS-BC with E_{GABA} set at -74 and -54 mV . **E:** summary data show effect of E_{GABA} on FS-BC firing during excitatory synaptic activation at 200 Hz at increasing FS-BC tonic g_{GABA} . Peak conductance of synaptic inputs was 20 nS .

post-SE FS-BC, and $10 \text{ } \mu\text{S}/\text{cm}^2$. Tonic g_{GABA} in model FS-BCs did not alter the background spontaneous activity (Fig. 11, A and C). Strikingly, while increasing FS-BC tonic g_{GABA} did not alter overall network excitability in response to focal afferent activation in some network instantiation (summarized in Fig. 11D as “low activity”), it significantly increased average granule cell firing and resulted in self-sustained, recurrent, seizure-like activity in a subset of simulated networks [Fig. 11A, summarized in Fig. 11D; between-subject analysis for effect of network structure: $F_{(1,11)} = 356.9$, $P < 0.05$ by univariate repeated-measures ANOVA]. Importantly, these results suggest that in the presence of a permissive network structure shunting tonic g_{GABA} augments network excitability, leading to seizure-like activity patterns (Fig. 11A). When the reversal potential of model FS-BC synaptic and tonic GABA currents was set to -54 mV , the background spontaneous activity was unchanged (Fig. 11, B and C). Notably, unlike simulations with

shunting E_{GABA} , networks simulated with depolarizing E_{GABA} showed no increase in evoked granule cell activity at all tonic g_{GABA} levels tested [Fig. 11, B and D; between-subject analysis for effect of E_{GABA} : $F_{(1,11)} = 345.3$, $P < 0.05$ by univariate repeated-measures ANOVA; interaction between network structure and E_{GABA} : $F_{(1,11)} = 355.2$, $P < 0.05$ by multivariate repeated-measures ANOVA]. To isolate the impact of FS-BC tonic g_{GABA} and E_{GABA} from network structural features, we set the randomization seed to a constant value to simulate structurally identical networks. Spike raster plots from simulations of structurally identical networks (illustrated in Fig. 11A) showed that when FS-BC E_{GABA} was -74 mV model networks had higher granule cell firing and recurrent network activity compared with networks with depolarizing (-54 mV) FS-BC E_{GABA} at all tonic g_{GABA} values tested. Next, we performed simulations on structurally identical networks (generated by 4 different predetermined randomization

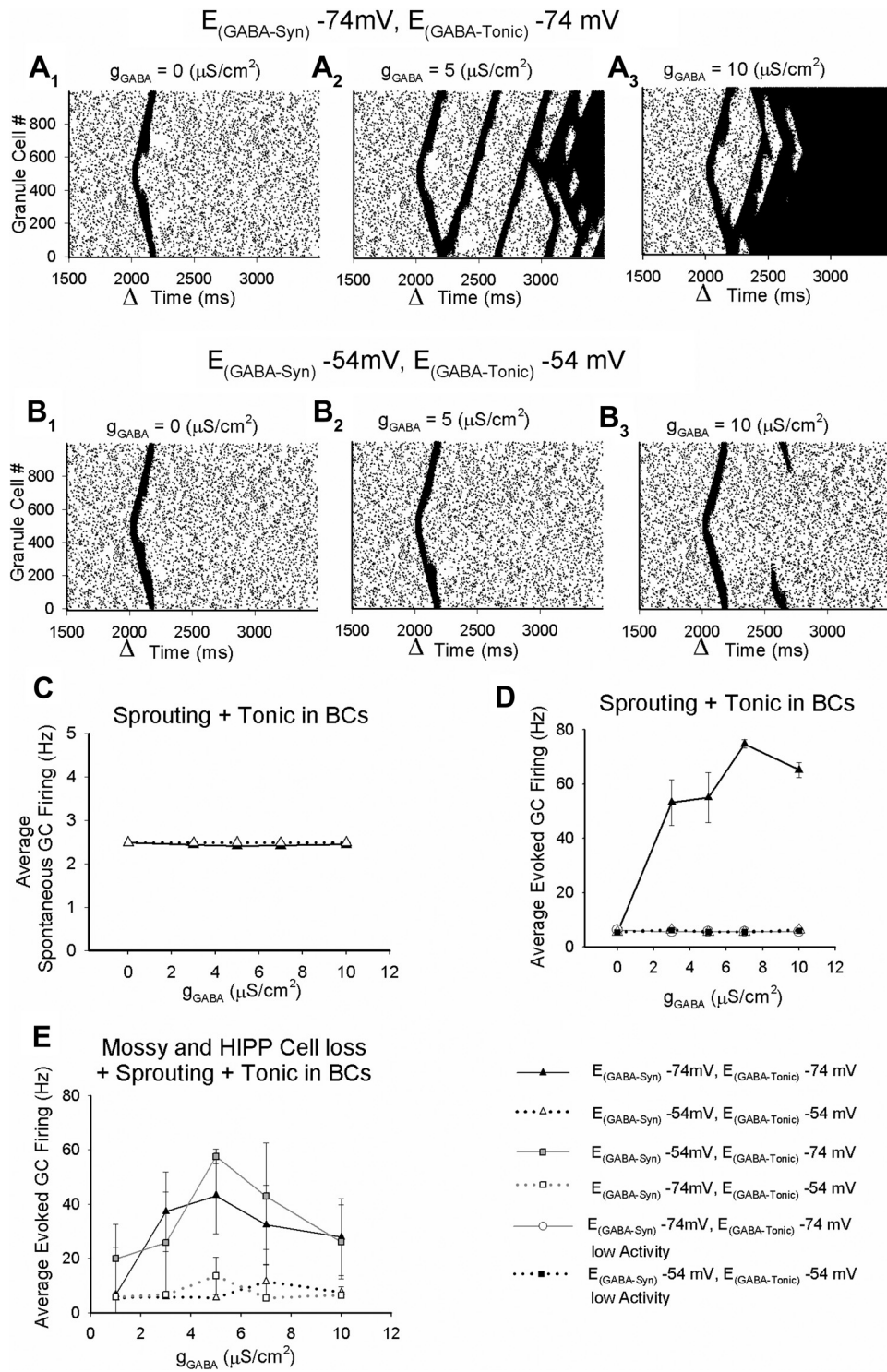


Fig. 11. Basket cell (BC) tonic GABAergic inhibition regulates dentate network excitability. **A:** granule cell (GC) spike rasters show the action potential firing of each of the 1,000 GCs. Each action potential is represented by a dot corresponding to the active cell (GC number on *y*-axis) at a certain simulation time (*x*-axis). Dentate networks were simulated as a ring with 20% sprouting. Network activity was established with Poisson-distributed suprathreshold inputs to granule cell dendrites at 2.5 Hz. A single synchronous suprathreshold activation of 100 GCs at the time marked by the arrowhead in each plot was used to simulate focal afferent activation. Spike rasters illustrate simulations performed with model FS-BC E_{GABA} at -74 mV , in the absence of tonic g_{GABA} (A_1), with $g_{\text{GABA}} = 5 \mu\text{S}/\text{cm}^2$ corresponding to a 30-pA FS-BC tonic I_{GABA} (A_2), and with $g_{\text{GABA}} = 10 \mu\text{S}/\text{cm}^2$ corresponding to a 60-pA tonic I_{GABA} (A_3). **B:** GC spikes form networks simulated as in **A**, with E_{GABA} in model FS-BCs set to -54 mV . GC spike rasters from simulations in the absence of tonic g_{GABA} (B_1), with $g_{\text{GABA}} = 5 \mu\text{S}/\text{cm}^2$ corresponding to a 30-pA FS-BC tonic I_{GABA} (B_2), and with $g_{\text{GABA}} = 10 \mu\text{S}/\text{cm}^2$ corresponding to a 60-pA tonic I_{GABA} (B_3) are illustrated. Spike rasters in **A** and **B** were derived from structurally identical network simulations. **C:** summary plots, on 3 runs in each condition, show the average spontaneous GC firing during 1,000–2,000 ms of the simulations as FS-BC tonic g_{GABA} was increased. **D:** summary of the average evoked GC firing during 2,001–3,500 ms of the simulation following focal afferent activation as a function of model FS-BC tonic g_{GABA} . Simulations were performed with E_{GABA} set at -74 mV or -54 mV (8 independent runs). Simulations in networks with “high activity” levels when E_{GABA} was -74 mV are summarized separately (4 runs at $E_{\text{GABA-Tonic}} = -74 \text{ mV}$ and 5 runs at $E_{\text{GABA-Tonic}} = -54 \text{ mV}$) from networks with low activity at both -74 mV and -54 mV E_{GABA} (5 runs each). **E:** summary of the average evoked GC firing following focal afferent activation as a function of model FS-BC tonic g_{GABA} in networks including mossy fiber sprouting and hilar neuronal loss. Simulations were conducted on 4 structurally identical networks showing high activity with tonic and synaptic E_{GABA} set at -74 mV . Key on right applies to **D** and **E**.

seed values that resulted in high-activity networks) including loss of dentate hilar neurons (mossy cells and HIPP cells) and mossy fiber sprouting. As in networks without cell loss, average granule cell firing was increased when FS-BC E_{GABA} was -74 mV and remained low when E_{GABA} was set to -54 mV (Fig. 11E). While our measurements of E_{GABA} during exogenous GABA application identified a post-SE depolarizing shift, given findings that the E_{GABA} within a neuron can differ between compartments (Baldi et al. 2010; Romo-Parra et al.

2008), it remains possible that synaptic GABA reversal may differ from the reversal of tonic I_{GABA} . In an additional simulation in which synaptic E_{GABA} was held either at -54 mV or at -74 mV independent of the E_{GABA} of the tonic g_{GABA} , networks with a depolarizing shift in the E_{GABA} of tonic g_{GABA} still consistently demonstrated lower excitability than identical networks with -74 mV tonic E_{GABA} [between-subject analysis for effect of tonic E_{GABA} : $F_{(1,11)} = 32.68$, $P < 0.05$; synaptic E_{GABA} : $F_{(1,11)} = 0.29$, $P > 0.05$; interaction

between tonic and synaptic E_{GABA} : $F_{(1,11)} = 0.46$, $P > 0.05$ by 2-way repeated-measures ANOVA]. Taken together, the simulations show that the depolarization of FS-BC E_{GABA} that occurs after SE can maintain FS-BC excitability despite increases in tonic g_{GABA} and could limit dentate network excitability after SE.

DISCUSSION

The ability of tonic GABAergic inhibition to regulate excitability of projection neurons suggests that tonic I_{GABA} may be modulated to prevent epileptogenesis (Meldrum and Rogawski 2007). Expression and seizure-induced changes in tonic I_{GABA} among dentate perisomatic interneurons critical for feedback inhibition can influence how modulating tonic inhibition will affect dentate function. Our study demonstrates that 1) GABA_AR δ-subunits, known to underlie tonic I_{GABA} , are expressed in PV+ interneurons in the hilar-granule cell layer border; 2) FS-BCs express tonic I_{GABA} that is enhanced 1 wk after SE; 3) increase in GABA_AR δ-subunit expression contributes to post-SE enhancement of FS-BC tonic I_{GABA} ; 4) in contrast to shunting GABAergic inhibition in controls, there is a positive shift in FS-BC E_{GABA} 1 wk after SE, resulting in a depolarizing driving force for I_{GABA} ; 5) corresponding to the post-SE depolarizing shift in FS-BC E_{GABA} , there is a reduction in the expression of the potassium-chloride cotransporter KCC2 in PV+ interneurons 1 wk after SE; and 6) in computational simulations incorporating tonic g_{GABA} in model FS-BCs, whereas shunting E_{GABA} reduces FS-BC firing and enhances dentate network excitability, depolarizing E_{GABA} reverses decreases in model FS-BC activity and prevents increases in network excitability.

Expression of tonic I_{GABA} in dentate FS-BCs. Perisomatically projecting interneurons expressing PV are critical for precision and timing of network activity (Freund 2003). Since tonic inhibition influences neuronal excitability, gain, and fidelity of information transmission (Duguid et al. 2012; Mitchell and Silver 2003; Song et al. 2011) and is additionally augmented by synaptic spillover during neuronal activity (Glykys and Mody 2007), FS-BC tonic I_{GABA} is ideally suited to regulate feedback inhibition and dentate throughput during behaviorally relevant neuronal activity. The ability of interneuronal tonic I_{GABA} to regulate gamma oscillations (Mann and Mody 2010) and the central role for FS-BCs in dentate gamma oscillations (Bartos et al. 2002) suggest that modulation of FS-BC tonic I_{GABA} by alcohol and neurosteroids, which act on GABA_ARs containing δ-subunits (Stell et al. 2003), may contribute to the impact of these drugs on memory function. Moreover, activity-dependent enhancement of FS-BC tonic I_{GABA} could provide the transient suppression of feedback inhibition needed to induce long-term potentiation in the dentate gyrus (Arima-Yoshida et al. 2011).

There are regional differences in the GABA_AR subunits mediating interneuronal tonic I_{GABA} , with α₅-subunits responsible for tonic I_{GABA} in CA1 interneurons and δ-subunits in CA3 and molecular layer interneurons (Glykys et al. 2007; Mann and Mody 2010; Semyanov et al. 2003). Unlike PV interneurons in the neocortex (Olah et al. 2009), and like molecular layer interneurons in the dentate (Glykys et al. 2007), we find that dentate PV interneurons express GABA_AR δ-subunits. Similar to fast-spiking interneurons in the murine neocortex (Krook-Magnuson et al. 2008), we show that tonic

I_{GABA} in dentate FS-BCs is modulated by a GABA_AR δ-subunit-specific agonist. Since dentate interneuron-like profiles show robust expression of GABA_AR α₁-subunits (Fritschy et al. 1999), and GABA_ARs containing α₁- and δ-subunits can mediate tonic I_{GABA} (Glykys et al. 2007), it is possible that GABA_ARs with α₁- and δ-subunits underlie FS-BC tonic I_{GABA} . Thus, although both granule cell and FS-BC tonic I_{GABA} are mediated by GABA_AR δ-subunits, differential contribution of α₁-subunits to FS-BC and α₄-subunits to granule cell tonic I_{GABA} may provide targets for cell-specific modulation of tonic inhibition.

SE-induced plasticity of FS-BC tonic inhibition. Perisomatic inhibition is pivotal in regulating granule cell excitability in both normal and epileptic dentate gyrus (Coulter and Carlson 2007; Kraushaar and Jonas 2000). Granule cell tonic I_{GABA} is known to be altered after SE (Rajasekaran et al. 2010; Zhan and Nadler 2009; Zhang et al. 2007). Since FS-BC tonic I_{GABA} is increased before the occurrence of behavioral seizures, and not as a compensatory response to changes in the epileptic network, FS-BC tonic I_{GABA} could play a role in development of epilepsy. Indeed, earlier studies have suggested that cellular and synaptic plasticity prior to the onset of spontaneous seizures contribute to epileptogenesis (Brooks-Kayal et al. 1998; Kobayashi et al. 2003; Pathak et al. 2007). Both increases in extracellular GABA due to synaptic spillover or compromised GABA transporter function and changes in GABA_AR expression could enhance tonic I_{GABA} (Farrant and Nusser 2005). However, sIPSC frequency in both FS-BCs (Fig. 6) and granule cells (Kobayashi and Buckmaster 2003) is reduced after SE, indicating that synaptic GABA spillover does not underlie the post-SE increases in FS-BC tonic I_{GABA} . Additionally, even when GABA transporters were blocked, post-SE FS-BCs had larger tonic I_{GABA} , indicating that factors other than compromises in GABA transporter function underlie the increase in tonic I_{GABA} . Our semiquantitative analyses demonstrate increase in the expression of GABA_AR δ-subunit in PV+ interneurons after SE. Although extensive efforts were taken to pair sections from control and experimental animals and to use identical methods during staining and imaging, admittedly quantification of immunofluorescence intensity is associated with limitations including nonlinear antigen-antibody reaction and changes in fluorescence arising from tissue properties and may not accurately reflect protein levels. Crucially, THIP, a GABA_AR δ-subunit-selective agonist under our experimental conditions (Brown et al. 2002; Gupta et al. 2012), causes greater baseline current shift in FS-BCs from post-SE rats, validating the semiquantitative immunofluorescence analysis and confirming that enhanced GABA_AR δ-subunit expression contributes to increases in FS-BC tonic I_{GABA} after SE. Thus the presence and SE-induced plasticity of FS-BC tonic I_{GABA} must be considered when developing seizure therapies targeting tonic inhibition.

Whether tonic I_{GABA} enhances or decreases neuronal excitability depends on complex interactions between GABA driving force and conductance (Song et al. 2011). Several studies have demonstrated that interneuronal E_{GABA} can provide shunting inhibition when E_{GABA} lies between RMP and action potential threshold (Banke and McBain 2006; Song et al. 2011; Vida et al. 2006). Consistent with earlier observations of shunting synaptic E_{GABA} in FS-BCs (Sauer and Bartos 2010; Vida et al. 2006), the difference between FS-BC RMP and

E_{GABA} determined during GABA application in controls was not significant. Methodological differences including use of whole cell recording conditions, younger animals, and CNQX, which unlike structurally related quinoxalinediones depolarizes hippocampal interneurons by nonspecific mechanisms (McBain et al. 1992), may have resulted in more depolarized RMP values in earlier studies (Geiger et al. 1997; Vida et al. 2006). It is important to note that the RMP values in our study are in the same range as the RMP of hippocampal interneurons measured with less invasive cell-attached recordings (Fricker et al. 1999; Verheugen et al. 1999). Moreover, RMP and E_{GABA} values in control FS-BCs in our study are similar to the RMP and IPSC reversal potential reported in hippocampal interneurons from animals over postnatal day 30 (Banke and McBain 2006) and likely result from developmental hyperpolarizing shift in interneuronal RMP and E_{GABA} (Banke and McBain 2006; Sauer and Bartos 2010). Importantly, we show that FS-BC E_{GABA} is depolarized relative to the RMP 1 wk after SE, resulting in a depolarizing GABA driving force, as previously reported in granule cells (Pathak et al. 2007). Curiously, despite post-SE changes in FS-BC I_{GABA} and E_{GABA} , FS-BC RMP remains unchanged. It is possible that changes in non-GABAergic ionic conductances compensate for changes in membrane conductance when tonic g_{GABA} is altered (Brickley et al. 2001). While the trauma of slicing can impact neuronal chloride homeostasis (Dzhala et al. 2012), our use of young adult animals and high-sucrose slicing solution minimizes these effects. Additionally, our inclusion of only morphologically intact neurons, the hyperpolarized FS-BC RMP, and the lack of difference between RMP in control and post-SE FS-BCs suggest that slicing-induced trauma is unlikely to underlie the post-SE depolarization of FS-BC E_{GABA} . FS-BC E_{GABA} undergoes a developmental hyperpolarizing shift believed to result from increases in the expression of the potassium-chloride cotransporter KCC2 (Sauer and Bartos 2010). While cognizant of the limitations of semiquantitative analysis of fluorescence intensity, we find consistent post-SE reduction in the intensity of membrane labeling for KCC2 in FS-BCs, suggesting that a decrease in KCC2 may contribute to the depolarizing shift in FS-BC E_{GABA} after SE. Whether FS-BCs, like granule cells (Pathak et al. 2007), show post-SE activity-dependent changes in the reversal potential for synaptic events remains to be tested.

Impact of tonic I_{GABA} and depolarizing E_{GABA} on FS-BC and network excitability. Using biophysically realistic multicompartmental FS-BC simulations, we determined the tonic conductance that modeled the experimentally observed FS-BC tonic I_{GABA} . Since recordings in slices at 33°C without added GABA or transporter antagonist likely underestimated tonic I_{GABA} amplitudes, our measurements with GABA transporter antagonists may better represent the magnitude of FS-BC tonic I_{GABA} in the biological tissue during neuronal activity. Voltage-clamp simulations identified the range of tonic g_{GABA} (1–10 $\mu\text{S}/\text{cm}^2$) that was compatible with experimentally derived estimates of FS-BC tonic I_{GABA} (10–60 pA). Changing tonic g_{GABA} across this entire range (50 pA) caused an $\sim 3.3\text{-M}\Omega$ shift in R_{in} and a <3% change in input conductance, suggesting that differences in R_{in} and input conductance due to a 10-pA shift in FS-BC tonic I_{GABA} may be difficult to detect experimentally. Increases in tonic g_{GABA} reduced model FS-BC excitability when E_{GABA} was -74 mV and, at similar

values of g_{GABA} , enhanced excitability when E_{GABA} was constrained by the depolarized values (-54 mV) observed after SE. As reported previously (Song et al. 2011), increasing tonic g_{GABA} beyond $1 \text{ mS}/\text{cm}^2$ in model FS-BCs resulted in shunting inhibition even with depolarizing E_{GABA} . However, the low FS-BC R_{in} and larger driving force (~ 20 mV) could account for the relatively high g_{GABA} needed to obtain shunting inhibition in our biophysically realistic FS-BC model compared with earlier simulations using single-compartment models with low-leak conductance (Song et al. 2011). Our simulations identify that, together, the post-SE changes in tonic I_{GABA} and E_{GABA} maintain FS-BC excitability during excitatory inputs (Fig. 10). It is possible that the parallel changes in tonic I_{GABA} and reversal potential reflect homeostatic plasticity to maintain FS-BC activity levels in the network (Howard et al. 2007; Turrigiano et al. 1994). In dentate network models with recurrent mossy fiber collaterals, including FS-BCs with simulated tonic I_{GABA} consistently resulted in low evoked granule cell activity when FS-BC E_{GABA} was depolarizing. Curiously, evoked granule cell activity in some but not all network implementations was greatly enhanced and developed into seizure-like recurrent firing when E_{GABA} was -74 mV. Since the average number of cell type-specific connections to each neuron in a given class of cells was not different between the networks, it is likely that the presence of a few highly connected hub cells and formation of feedback excitatory loops (Morgan and Soltesz 2008) may have contributed to the differences in activity patterns between the networks with otherwise identical connectivity statistics. While our simulations predict that post-SE changes in FS-BC inhibition can limit early SE-induced increases in dentate excitability when sprouting is low, structural reorganization and cell loss associated with epileptogenesis could undermine this potential compensatory mechanism. Additionally, maintenance of normal neuronal and network excitability despite altered g_{GABA} and reversal is consistent with recent studies suggesting that multiple combinations of intrinsic parameters can result in similar circuit performance (Marder 2011). However, all parameter combinations may not be identically robust in maintaining normal activity during different network perturbations. Thus, while the observed changes in tonic I_{GABA} and E_{GABA} maintain normal FS-BC and dentate activity during focal afferent activation, these changes may compromise FS-BC responses during certain patterns of network perturbations and may impact generation of network rhythms contributing to memory impairments associated with seizure disorders.

ACKNOWLEDGMENTS

We thank Dr. Jamie Magurie for the gift of $\text{GABA}_{\text{AR}}\delta^{-/-}$ mouse brains and Drs. Josh Berlin, Stella Elkabes, and Robert F. Heary for equipment and discussions.

GRANTS

This work is supported by an Epilepsy Foundation Research Grant and National Institute of Neurological Disorders and Stroke Grant NS-069861 to V. Santhakumar.

DISCLOSURES

No conflicts of interest, financial or otherwise, are declared by the author(s).

AUTHOR CONTRIBUTIONS

Author contributions: J.Y., A.P., and T.I. performed experiments; J.Y., A.P., and F.S.E. analyzed data; J.Y., A.P., and V.S. interpreted results of experiments; J.Y., A.P., and F.S.E. prepared figures; J.Y., A.P., F.S.E., T.I., and V.S. approved final version of manuscript; F.S.E. and V.S. edited and revised manuscript; V.S. conception and design of research; V.S. drafted manuscript.

REFERENCES

- Arima-Yoshida F, Watabe AM, Manabe T.** The mechanisms of the strong inhibitory modulation of long-term potentiation in the rat dentate gyrus. *Eur J Neurosci* 33: 1637–1646, 2011.
- Baldi R, Varga C, Tamas G.** Differential distribution of KCC2 along the axo-somato-dendritic axis of hippocampal principal cells. *Eur J Neurosci* 32: 1319–1325, 2010.
- Banker TG, McBain CJ.** GABAergic input onto CA3 hippocampal interneurons remains shunting throughout development. *J Neurosci* 26: 11720–11725, 2006.
- Bartos M, Vida I, Frotscher M, Geiger JR, Jonas P.** Rapid signaling at inhibitory synapses in a dentate gyrus interneuron network. *J Neurosci* 21: 2687–2698, 2001.
- Bartos M, Vida I, Frotscher M, Meyer A, Monyer H, Geiger JR, Jonas P.** Fast synaptic inhibition promotes synchronized gamma oscillations in hippocampal interneuron networks. *Proc Natl Acad Sci USA* 99: 13222–13227, 2002.
- Ben-Ari Y.** Developing networks play a similar melody. *Trends Neurosci* 24: 353–360, 2001.
- Bianchi MT, Macdonald RL.** Agonist trapping by GABA_A receptor channels. *J Neurosci* 21: 9083–9091, 2001.
- Billups D, Attwell D.** Control of intracellular chloride concentration and GABA response polarity in rat retinal ON bipolar cells. *J Physiol* 545: 183–198, 2002.
- Bragin A, Wilson CL, Almajano J, Mody I, Engel J Jr.** High-frequency oscillations after status epilepticus: epileptogenesis and seizure genesis. *Epilepsia* 45: 1017–1023, 2004.
- Brickley SG, Revilla V, Cull-Candy SG, Wisden W, Farrant M.** Adaptive regulation of neuronal excitability by a voltage-independent potassium conductance. *Nature* 409: 88–92, 2001.
- Brooks-Kayal AR, Shumate MD, Jin H, Rikhter TY, Coulter DA.** Selective changes in single cell GABA_A receptor subunit expression and function in temporal lobe epilepsy. *Nat Med* 4: 1166–1172, 1998.
- Brown N, Kerby J, Bonnert TP, Whiting PJ, Wafford KA.** Pharmacological characterization of a novel cell line expressing human alpha₄beta₃delta GABA_A receptors. *Br J Pharmacol* 136: 965–974, 2002.
- Buckmaster PS, Yamawaki R, Zhang GF.** Axon arbors and synaptic connections of a vulnerable population of interneurons in the dentate gyrus *in vivo*. *J Comp Neurol* 445: 360–373, 2002.
- Buzsaki G.** *Rhythms of the Brain*. New York: Oxford Univ. Press, 2006.
- Cossart R, Bernard C, Ben-Ari Y.** Multiple facets of GABAergic neurons and synapses: multiple fates of GABA signalling in epilepsies. *Trends Neurosci* 28: 108–115, 2005.
- Coulter DA.** Epilepsy-associated plasticity in gamma-aminobutyric acid receptor expression, function, and inhibitory synaptic properties. *Int Rev Neurobiol* 45: 237–252, 2001.
- Coulter DA, Carlson GC.** Functional regulation of the dentate gyrus by GABA-mediated inhibition. *Prog Brain Res* 163: 235–243, 2007.
- Duguid I, Branco T, London M, Chadderton P, Häusser M.** Tonic inhibition enhances fidelity of sensory information transmission in the cerebellar cortex. *J Neurosci* 32: 11132–11143, 2012.
- Dyhrfjeld-Johnsen J, Santhakumar V, Morgan RJ, Huerta R, Tsimring L, Soltesz I.** Topological determinants of epileptogenesis in large-scale structural and functional models of the dentate gyrus derived from experimental data. *J Neurophysiol* 97: 1566–1587, 2007.
- Dzhala V, Valeeva G, Glykys J, Khazipov R, Staley K.** Traumatic alterations in GABA signaling disrupt hippocampal network activity in the developing brain. *J Neurosci* 32: 4017–4031, 2012.
- Ebihara S, Shirato K, Harata N, Akaike N.** Gramicidin-perforated patch recording: GABA response in mammalian neurones with intact intracellular chloride. *J Physiol* 484: 77–86, 1995.
- Ekstrand JJ, Pouliot W, Scheerlinck P, Dudek FE.** Lithium pilocarpine-induced status epilepticus in postnatal day 20 rats results in greater neuronal injury in ventral versus dorsal hippocampus. *Neuroscience* 192: 699–707, 2011.
- Ewell LA, Jones MV.** Frequency-tuned distribution of inhibition in the dentate gyrus. *J Neurosci* 30: 12597–12607, 2010.
- Farrant M, Nusser Z.** Variations on an inhibitory theme: phasic and tonic activation of GABA_A receptors. *Nat Rev Neurosci* 6: 215–229, 2005.
- Freund TF.** Interneuron Diversity series: Rhythm and mood in perisomatic inhibition. *Trends Neurosci* 26: 489–495, 2003.
- Fricker D, Verheugen JA, Miles R.** Cell-attached measurements of the firing threshold of rat hippocampal neurones. *J Physiol* 517: 791–804, 1999.
- Fritschy JM, Kiener T, Bouilleret V, Loup F.** GABAergic neurons and GABA_A-receptors in temporal lobe epilepsy. *Neurochem Int* 34: 435–445, 1999.
- Geiger JR, Lubke J, Roth A, Frotscher M, Jonas P.** Submillisecond AMPA receptor-mediated signaling at a principal neuron-interneuron synapse. *Neuron* 18: 1009–1023, 1997.
- Glykys J, Mody I.** The main source of ambient GABA responsible for tonic inhibition in the mouse hippocampus. *J Physiol* 582: 1163–1178, 2007.
- Glykys J, Peng Z, Chandra D, Homann GE, Houser CR, Mody I.** A new naturally occurring GABA_A receptor subunit partnership with high sensitivity to ethanol. *Nat Neurosci* 10: 40–48, 2007.
- Gupta A, Elgammal FS, Produttori A, Shah S, Santhakumar V.** Decrease in tonic inhibition contributes to increase in dentate semilunar granule cell. *J Neurosci* 32: 2523–2537, 2012.
- Harney SC, Jones MV.** Pre- and postsynaptic properties of somatic and dendritic inhibition in dentate gyrus. *Neuropharmacology* 43: 584–594, 2002.
- Hefft S, Jonas P.** Asynchronous GABA release generates long-lasting inhibition at a hippocampal interneuron-principal neuron synapse. *Nat Neurosci* 8: 1319–1328, 2005.
- Hines ML, Carnevale NT.** The NEURON simulation environment. *Neural Comput* 9: 1179–1209, 1997.
- Howard AL, Neu A, Morgan RJ, Echegoyen JC, Soltesz I.** Opposing modifications in intrinsic currents and synaptic inputs in post-traumatic mossy cells: evidence for single-cell homeostasis in a hyperexcitable network. *J Neurophysiol* 97: 2394–2409, 2007.
- Kobayashi M, Buckmaster PS.** Reduced inhibition of dentate granule cells in a model of temporal lobe epilepsy. *J Neurosci* 23: 2440–2452, 2003.
- Kobayashi M, Wen X, Buckmaster PS.** Reduced inhibition and increased output of layer II neurons in the medial entorhinal cortex in a model of temporal lobe epilepsy. *J Neurosci* 23: 8471–8479, 2003.
- Kraushaar U, Jonas P.** Efficacy and stability of quantal GABA release at a hippocampal interneuron-principal neuron synapse. *J Neurosci* 20: 5594–5607, 2000.
- Krook-Magnuson EI, Li P, Paluszakiewicz SM, Huntsman MM.** Tonically active inhibition selectively controls feedforward circuits in mouse barrel cortex. *J Neurophysiol* 100: 932–944, 2008.
- Mann EO, Mody I.** Control of hippocampal gamma oscillation frequency by tonic inhibition and excitation of interneurons. *Nat Neurosci* 13: 205–212, 2010.
- Marder E.** Variability, compensation, and modulation in neurons and circuits. *Proc Natl Acad Sci USA* 108, Suppl 3: 15542–15548, 2011.
- Margerison JH, Corsellis JA.** Epilepsy and the temporal lobes. A clinical, electroencephalographic and neuropathological study of the brain in epilepsy, with particular reference to the temporal lobes. *Brain* 89: 499–530, 1966.
- McBain CJ, Eaton JV, Brown T, Dingledine R.** CNQX increases spontaneous inhibitory input to CA3 pyramidal neurones in neonatal rat hippocampal slices. *Brain Res* 592: 255–260, 1992.
- Meldrum BS, Rogawski MA.** Molecular targets for antiepileptic drug development. *Neurotherapeutics* 4: 18–61, 2007.
- Mello LE, Cavalheiro EA, Tan AM, Kupfer WR, Pretorius JK, Babb TL, Finch DM.** Circuit mechanisms of seizures in the pilocarpine model of chronic epilepsy: cell loss and mossy fiber sprouting. *Epilepsia* 34: 985–995, 1993.
- Mitchell SJ, Silver RA.** Shunting inhibition modulates neuronal gain during synaptic excitation. *Neuron* 38: 433–445, 2003.
- Morgan RJ, Soltesz I.** Nonrandom connectivity of the epileptic dentate gyrus predicts a major role for neuronal hubs in seizures. *Proc Natl Acad Sci USA* 105: 6179–6184, 2008.
- Mtchedlishvili Z, Kapur J.** High-affinity, slowly desensitizing GABA_A receptors mediate tonic inhibition in hippocampal dentate granule cells. *Mol Pharmacol* 69: 564–575, 2006.
- Olah S, Fule M, Komlosi G, Varga C, Baldi R, Barzo P, Tamas G.** Regulation of cortical microcircuits by unitary GABA-mediated volume transmission. *Nature* 461: 1278–1281, 2009.

- Pathak HR, Weissinger F, Terunuma M, Carlson GC, Hsu FC, Moss SJ, Coulter DA.** Disrupted dentate granule cell chloride regulation enhances synaptic excitability during development of temporal lobe epilepsy. *J Neurosci* 27: 14012–14022, 2007.
- Peng Z, Huang CS, Stell BM, Mody I, Houser CR.** Altered expression of the delta subunit of the GABA_A receptor in a mouse model of temporal lobe epilepsy. *J Neurosci* 24: 8629–8639, 2004.
- Rajasekaran K, Joshi S, Sun C, Mtchedlishvili Z, Kapur J.** Receptors with low affinity for neurosteroids and GABA contribute to tonic inhibition of granule cells in epileptic animals. *Neurobiol Dis* 40: 490–501, 2010.
- Rao YS, Budreck EC, Brooks-Kayal AR.** Epilepsy after early-life seizures can be independent of hippocampal injury. *Ann Neurol* 53: 503–511, 2003.
- Rivera C, Voipio J, Kaila K.** Two developmental switches in GABAergic signalling: the K⁺-Cl⁻ cotransporter KCC2 and carbonic anhydrase CAVII. *J Physiol* 562: 27–36, 2005.
- Romo-Parra H, Trevino M, Heinemann U, Gutierrez R.** GABA actions in hippocampal area CA3 during postnatal development: differential shift from depolarizing to hyperpolarizing in somatic and dendritic compartments. *J Neurophysiol* 99: 1523–1534, 2008.
- Rossi DJ, Hamann M, Attwell D.** Multiple modes of GABAergic inhibition of rat cerebellar granule cells. *J Physiol* 548: 97–110, 2003.
- Santhakumar V.** Modeling mossy cell loss and mossy fiber sprouting in epilepsy. In: *Computational Neuroscience in Epilepsy*, edited by Soltesz I, Staley KJ. San Diego, CA: Academic, 2008, p. 89–111.
- Santhakumar V, Aradi I, Soltesz I.** Role of mossy fiber sprouting and mossy cell loss in hyperexcitability: a network model of the dentate gyrus incorporating cell types and axonal topography. *J Neurophysiol* 93: 437–453, 2005.
- Santhakumar V, Bender R, Frotscher M, Ross ST, Hollrigel GS, Toth Z, Soltesz I.** Granule cell hyperexcitability in the early post-traumatic rat dentate gyrus: the “irritable mossy cell” hypothesis. *J Physiol* 524: 117–134, 2000.
- Santhakumar V, Hanchar HJ, Wallner M, Olsen RW, Otis TS.** Contributions of the GABA_A receptor alpha6 subunit to phasic and tonic inhibition revealed by a naturally occurring polymorphism in the alpha6 gene. *J Neurosci* 26: 3357–3364, 2006.
- Santhakumar V, Jones RT, Mody I.** Developmental regulation and neuroprotective effects of striatal tonic GABA_A currents. *Neuroscience* 167: 644–655, 2010.
- Santhakumar V, Ratzliff AD, Jeng J, Toth K, Soltesz I.** Long-term hyperexcitability in the hippocampus after experimental head trauma. *Ann Neurol* 50: 708–717, 2001.
- Sauer JF, Bartos M.** Recruitment of early postnatal parvalbumin-positive hippocampal interneurons by GABAergic excitation. *J Neurosci* 30: 110–115, 2010.
- Scimemi A, Semyanov A, Sperk G, Kullmann DM, Walker MC.** Multiple and plastic receptors mediate tonic GABA_A receptor currents in the hippocampus. *J Neurosci* 25: 10016–10024, 2005.
- Semyanov A, Walker MC, Kullmann DM.** GABA uptake regulates cortical excitability via cell type-specific tonic inhibition. *Nat Neurosci* 6: 484–490, 2003.
- Song I, Savchenko L, Semyanov A.** Tonic excitation or inhibition is set by GABA_A conductance in hippocampal interneurons. *Nat Commun* 2: 376, 2011.
- Stell BM, Brickley SG, Tang CY, Farrant M, Mody I.** Neuroactive steroids reduce neuronal excitability by selectively enhancing tonic inhibition mediated by delta subunit-containing GABA_A receptors. *Proc Natl Acad Sci USA* 100: 14439–14444, 2003.
- Turrigiano G, Abbott LF, Marder E.** Activity-dependent changes in the intrinsic properties of cultured neurons. *Science* 264: 974–977, 1994.
- Verheugen JA, Fricker D, Miles R.** Noninvasive measurements of the membrane potential and GABAergic action in hippocampal interneurons. *J Neurosci* 19: 2546–2555, 1999.
- Vida I, Bartos M, Jonas P.** Shunting inhibition improves robustness of gamma oscillations in hippocampal interneuron networks by homogenizing firing rates. *Neuron* 49: 107–117, 2006.
- Wei W, Zhang N, Peng Z, Houser CR, Mody I.** Perisynaptic localization of delta subunit-containing GABA_A receptors and their activation by GABA spillover in the mouse dentate gyrus. *J Neurosci* 23: 10650–10661, 2003.
- West MJ, Slomianka L, Gundersen HJ.** Unbiased stereological estimation of the total number of neurons in the subdivisions of the rat hippocampus using the optical fractionator. *Anat Rec* 231: 482–497, 1991.
- Zhan RZ, Nadler JV.** Enhanced tonic GABA current in normotopic and hilar ectopic dentate granule cells after pilocarpine-induced status epilepticus. *J Neurophysiol* 102: 670–681, 2009.
- Zhang N, Wei W, Mody I, Houser CR.** Altered localization of GABA_A receptor subunits on dentate granule cell dendrites influences tonic and phasic inhibition in a mouse model of epilepsy. *J Neurosci* 27: 7520–7531, 2007.
- Zhang W, Buckmaster PS.** Dysfunction of the dentate basket cell circuit in a rat model of temporal lobe epilepsy. *J Neurosci* 29: 7846–7856, 2009.
- Zhang W, Huguenard JR, Buckmaster PS.** Increased excitatory synaptic input to granule cells from hilar and CA3 regions in a rat model of temporal lobe epilepsy. *J Neurosci* 32: 1183–1196, 2012.
- Zhang W, Yamawaki R, Wen X, Uhl J, Diaz J, Prince DA, Buckmaster PS.** Surviving hilar somatostatin interneurons enlarge, sprout axons, and form new synapses with granule cells in a mouse model of temporal lobe epilepsy. *J Neurosci* 29: 14247–14256, 2009.